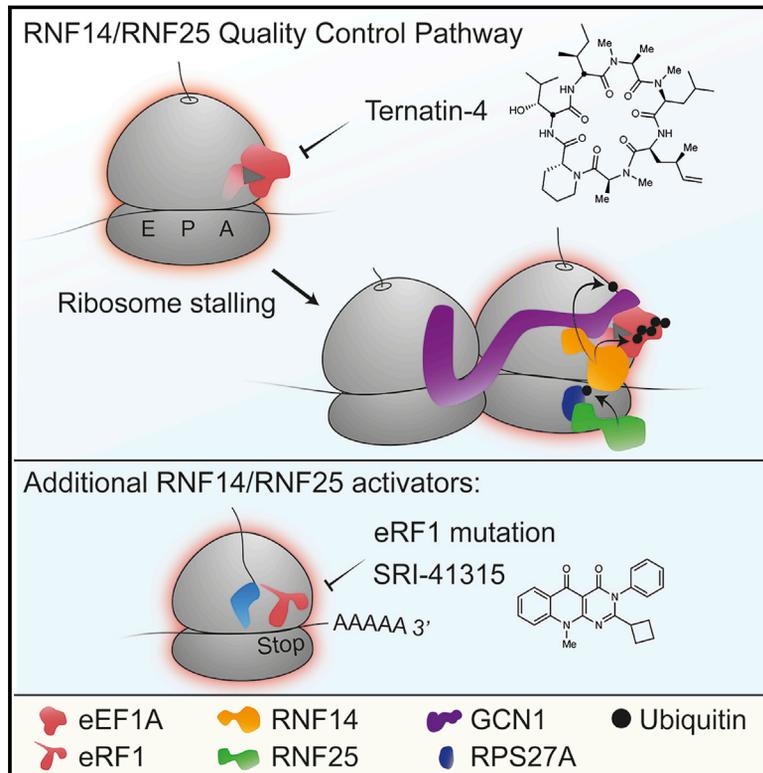# An E3 ligase network engages GCN1 to promote the degradation of translation factors on stalled ribosomes

Graphical abstract

Authors

Keely Oltion, Jordan D. Carelli, Tangpo Yang, Stephanie K. See, Hao-Yuan Wang, Martin Kampmann, Jack Taunton

Correspondence

jack.taunton@ucsf.edu

In brief

Oltion et al. unveil a ubiquitin ligase network in charge of ensuring translation factor quality control in response to stalled ribosomes.

Highlights

- Cellular response to ternatin-4 unveils the RNF14/RNF25 translation quality control pathway

- Ternatin-4 traps eEF1A/aa-tRNA at the ribosome A site, triggering eEF1A degradation

- RNF25 ubiquitination of RPS27A and RNF14/GCN1 binding lead to eEF1A ubiquitination by RNF14

- Stalled eRF1 is also targeted for degradation by the RNF14/RNF25 pathway

Cell

CellPress

Article

An E3 ligase network engages GCN1 to promote the degradation of translation factors on stalled ribosomes

Keely Oltion,[1] Jordan D. Carelli,[1] Tangpo Yang,[2] Stephanie K. See,[1] Hao-Yuan Wang,[2] Martin Kampmann,[3,4] and Jack Taunton[2,5,*]

[1]Chemistry and Chemical Biology Graduate Program, University of California, San Francisco, San Francisco, CA 94158, USA
[2]Department of Cellular and Molecular Pharmacology, University of California, San Francisco, San Francisco, CA 94158, USA
[3]Institute for Neurodegenerative Diseases, Department of Biochemistry and Biophysics, University of California, San Francisco, San Francisco, CA 94158, USA
[4]Chan Zuckerberg Biohub, San Francisco, CA 94158, USA
[5]Lead contact
*Correspondence: jack.taunton@ucsf.edu
https://doi.org/10.1016/j.cell.2022.12.025

SUMMARY

Ribosomes frequently stall during mRNA translation, resulting in the context-dependent activation of quality control pathways to maintain proteostasis. However, surveillance mechanisms that specifically respond to stalled ribosomes with an occluded A site have not been identified. We discovered that the elongation factor-1α (eEF1A) inhibitor, ternatin-4, triggers the ubiquitination and degradation of eEF1A on stalled ribosomes. Using a chemical genetic approach, we unveiled a signaling network comprising two E3 ligases, RNF14 and RNF25, which are required for eEF1A degradation. Quantitative proteomics revealed the RNF14 and RNF25-dependent ubiquitination of eEF1A and a discrete set of ribosomal proteins. The ribosome collision sensor GCN1 plays an essential role by engaging RNF14, which directly ubiquitinates eEF1A. The site-specific, RNF25-dependent ubiquitination of the ribosomal protein RPS27A/eS31 provides a second essential signaling input. Our findings illuminate a ubiquitin signaling network that monitors the ribosomal A site and promotes the degradation of stalled translation factors, including eEF1A and the termination factor eRF1.

INTRODUCTION

Protein synthesis is essential for growth and survival in all organisms. Each stage of protein synthesis, including initiation, elongation, and termination, is choreographed by factors that interact with the central catalytic machinery—the ribosome.[1] The initiation stage, often rate limiting for protein production, is tightly regulated by cellular signaling pathways.[2,3] We know less about how cells regulate elongation rates, which are highly variable across coding sequences. Such regulation underlies, for example, the dependence of elongation rates on peptide sequence, codon usage, tRNA expression, and post-transcriptional modifications of tRNA and mRNA.[4,5] As a consequence, ribosomes may pause or stall in a context-dependent manner, and this may be critical for optimal folding or the subcellular targeting of a nascent polypeptide.[6]

Ribosome stalling can also result from the attempted translation of a defective mRNA.[7,8] Such pathological stalls can lead to proteotoxic stress caused by the depletion of active ribosomes and the accumulation of partially synthesized nascent polypeptides. Experiments monitoring the translation of mRNA reporters with poly(A) and other stall-prone coding sequences have revealed surveillance pathways that recognize distinct structural features.[8] The HBS1L/PELO complex recognizes the empty ribosomal A site at the 3′ end of a truncated mRNA and promotes ribosome splitting by the recycling factor ABCE1.[9,10] By contrast, attempted translation of poly(A) slows down a leading ribosome to the point that a trailing ribosome collides, resulting in Hel2/ZNF598-mediated ubiquitination of 40S ribosomal proteins and subunit dissociation by the ribosome-associated quality control (RQC)-triggering (RQT) complex.[11–17] An emerging view posits that ribosome collisions comprise a fundamental structural unit recognized by multiple quality control and stress response factors,[18,19] including the E3 ligase, Hel2/ZNF598, and the integrated stress response coactivator, GCN1.[20] Although these translation surveillance pathways were identified in budding yeast more than 10 years ago, the elucidation of their physiological roles in mammalian systems has only just begun. Moreover, it is currently unknown whether there are additional surveillance pathways that specifically respond to stalled ribosomes occupied by translation factors, such as elongation factor-1α (eEF1A) or termination factors (eRF1 and eRF3).
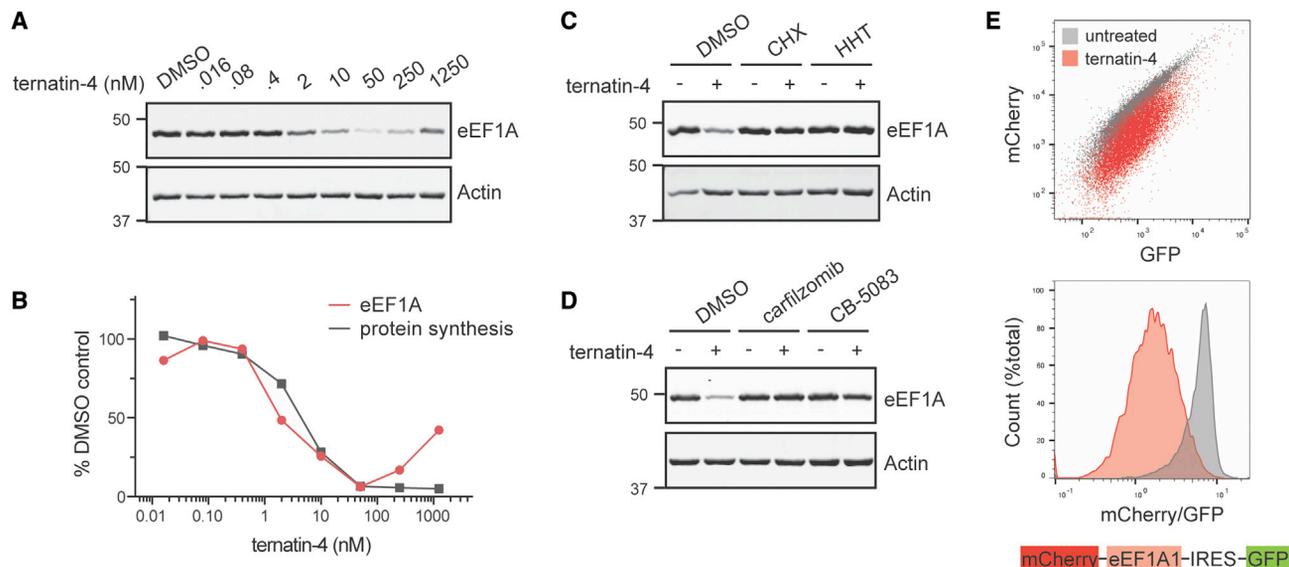
Figure 1. Ternatin-4 promotes eEF1A degradation in a manner that requires translating ribosomes

(A) HeLa cells were treated with ternatin-4 for 20 h.

(B) Quantification of eEF1A levels is derived from (A). Protein synthesis was measured after 20 h ternatin-4 treatment by pulsing cells with O-propargyl puromycin for 1 h and analyzed by flow cytometry (see STAR Methods).

(C) HeLa cells were treated with ternatin-4 (50 nM) for 20 h in the presence or absence of cycloheximide (CHX, 50 μg/mL) or homoharringtonine (HHT, 2 μg/mL, 20 min pretreatment).

(D) HeLa cells were treated for 20 h with ternatin-4 (50 nM) in the presence or absence of the proteasome inhibitor, carfilzomib (500 nM), or the p97 inhibitor, CB-5083 (2.5 μM).

(E) Fluorescent reporter to monitor eEF1A degradation. Ternatin-resistant HCT116 cells (eEF1A1$^{A399V/A339V}$) stably expressing mCherry-eEF1A1_IRES-GFP and dCas9 were treated ±ternatin-4 (50 nM) for 8 h and analyzed by flow cytometry.

See also Figure S1.

Studies of translation quality control have critically relied on the use of drugs and chemical probes to modulate protein synthesis in a graded, dose-dependent manner.[11,12,16,21,22] We recently described ternatin-4, a small-molecule inhibitor of translation elongation that targets the complex of eEF1A bound to aminoacyl-tRNAs (aa-tRNA).[23] Similar to didemnin B,[24] ternatin-4 stalls elongation by preventing aa-tRNA release from eEF1A on the ribosome.[25,26] Based on this mechanism, we reasoned that ternatin-4 could be used as a tool to illuminate the cellular response to elongation-stalled ribosomes in which the A site is persistently occupied by eEF1A bound to aa-tRNA.

Here, we elucidate a surveillance pathway that ultimately results in the ubiquitination and degradation of eEF1A trapped on the ribosome by ternatin-4. A CRISPRi screen uncovered two poorly characterized E3 ligases, RNF14 and RNF25, both of which are required for ternatin-induced eEF1A degradation. In response to ternatin-induced stalls, RNF14 and RNF25 play essential roles in the ubiquitination of eEF1A, as well as multiple ribosomal proteins. The ubiquitination of the ribosomal protein RPS27A is mediated solely by RNF25 and is required for eEF1A degradation. We further show that GCN1—whose biological roles beyond the canonical integrated stress response are poorly understood—interacts with RNF14 and is also essential for eEF1A degradation. We propose that the RNF14/RNF25 surveillance network—which we find also targets the eukaryotic release factor eRF1—monitors the status of elongating and ter-

minating ribosomes and specifically responds to stalls containing an occluded A site.

RESULTS

Ternatin-4 promotes eEF1A degradation in a manner that requires translating ribosomes

In experiments evaluating the cellular response to ternatin-induced elongation stalls, we unexpectedly observed a sharp reduction in eEF1A levels (Figure 1A). The loss of eEF1A was dependent on the concentration of ternatin-4, with an effective half-maximal concentration (EC$_{50}$) of ~8 nM. We noted that concentrations higher than 50 nM had progressively diminished effects on eEF1A levels, despite effectively inhibiting translation (Figure 1B). This dose-response behavior is reminiscent of mechanistically distinct elongation inhibitors (e.g., cycloheximide [CHX], emetine, and anisomycin) in which intermediate but not high concentrations were found to activate ribosome quality control and stress kinase pathways by promoting ribosome collisions.[12,16,21] Based on these precedents and the observed "V-shaped" dose-response curve (Figure 1B), it seemed plausible that intermediate concentrations of ternatin-4 could induce ribosome collisions and, ultimately, eEF1A degradation. Consistent with this notion, treatment with ternatin-4 for 1 h led to an increase in the proportion of nuclease-resistant disomes and trisomes (Figure S1A).
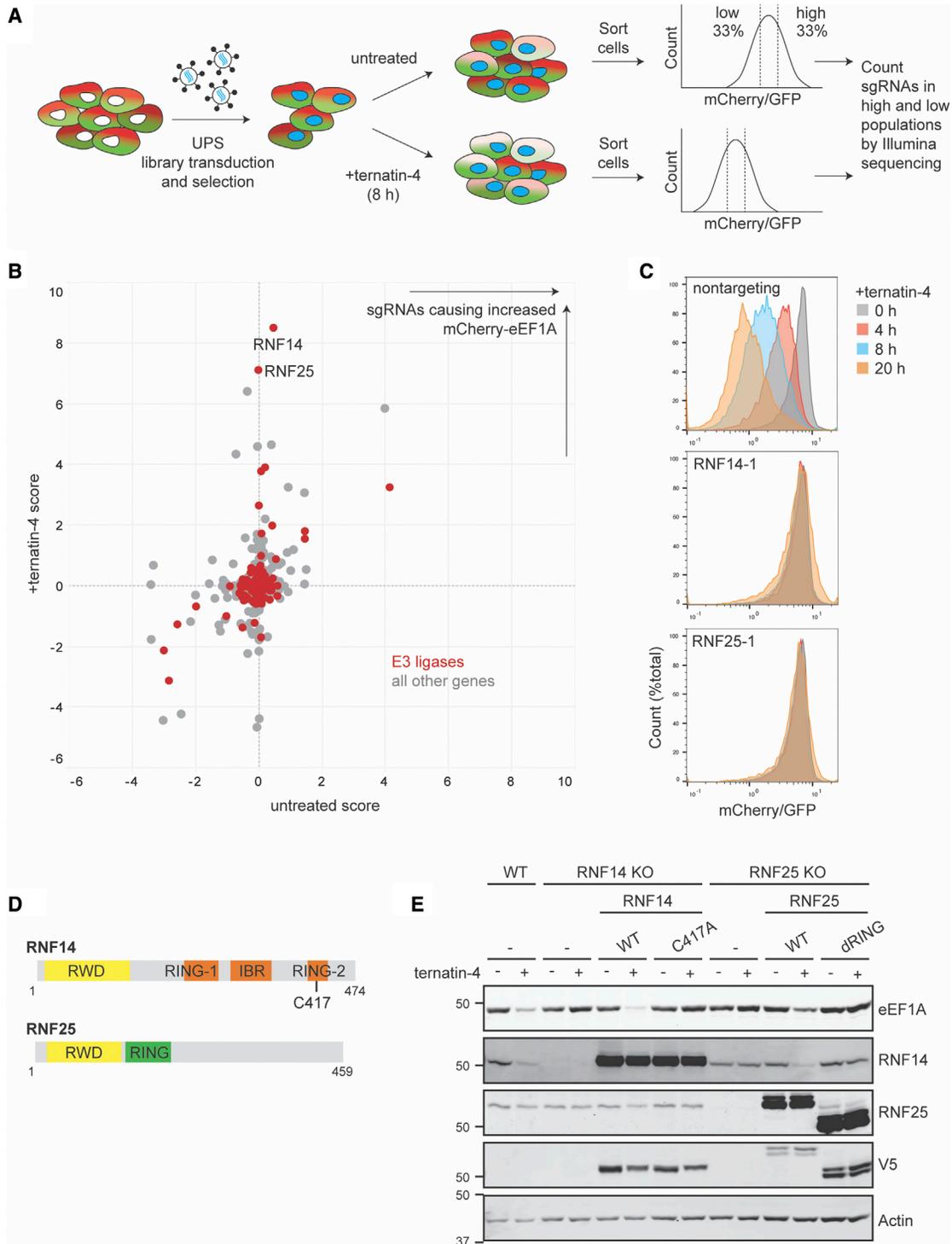
Figure 2. CRISPRi screen reveals two E3 ligases required for ternatin-induced eEF1A degradation

(A) Schematic of CRISPRi screen. CRISPRi reporter cells from Figure 1E were transduced with a library targeting ~1,700 genes (5 sgRNAs/gene) related to ubiquitin signaling and proteostasis. sgRNA-expressing cells were treated with ternatin-4 for 8 h or left untreated. Cells were sorted into high and low mCherry/GFP populations, and sgRNA counts were determined by deep sequencing.

(B) Knockdown of *RNF14* or *RNF25* stabilizes mCherry-eEF1A1 levels in ternatin-treated but not untreated cells. CRISPRi scores are plotted for each gene and are the product of the phenotype value ($\log_2$ of the average high/low sgRNA counts for the three most extreme sgRNAs per gene) and the negative $\log_{10}$ of the p value.

(legend continued on next page)

eEF1A is one of the most abundant cellular proteins ($\sim$35 μM in cells) and has been reported to turn over slowly.[27] In contrast to results obtained with ternatin-4, treatment of HeLa cells for 20 h with CHX or homoharringtonine (HHT) had no effect on eEF1A levels (Figure 1C). Hence, inhibiting translation per se is not sufficient to promote the loss of eEF1A; rather, the direct binding of ternatin-4 to eEF1A on the ribosome might be required. In support of this hypothesis, co-treatment with ternatin-4 and either CHX or HHT—which target the ribosomal E site and peptidyltransferase center, respectively—completely prevented eEF1A degradation (Figure 1C). These results suggest that ternatin-induced eEF1A degradation requires actively translating ribosomes that are competent to bind eEF1A/aa-tRNA. Such ribosomes would be less abundant in cells treated with CHX or HHT owing to their inhibitory effects on mRNA-tRNA translocation and initiation, respectively.[28,29] Ternatin-induced eEF1A degradation was also prevented by co-treatment with either proteasome or p97/VCP inhibitors (Figure 1D), thus implicating the ubiquitin/proteasome system (UPS) in this process. Collectively, our findings suggest that ternatin-4, which traps eEF1A on the ribosome and prevents aa-tRNA accommodation into the A site,[25,26] targets eEF1A for UPS-mediated destruction by a mechanism that requires elongation-competent ribosomes.

CRISPRi screen reveals two E3 ligases required for ternatin-induced eEF1A degradation

We sought to identify the UPS components and, in particular, the E3 ligase(s) required for ternatin-induced eEF1A degradation. To do this, we performed a CRISPRi screen using an mCherry-eEF1A fusion as a fluorescent reporter, which also contains an internal ribosome entry site (IRES) followed by GFP. We stably expressed this bicistronic reporter construct, along with dCas9-BFP-KRAB, in HCT116 cells that are homozygous for an A399V mutation in the didemnin/ternatin-4 binding site of eEF1A1. We previously showed that this mutation abrogates ternatin-4 binding and confers complete resistance to its cellular effects.[23] Hence, this reporter cell line, which expresses mCherry-eEF1A at low levels relative to endogenous A399V eEF1A, allows us to study ternatin-induced eEF1A degradation without globally inhibiting protein synthesis. Treatment of the reporter cells with ternatin-4 resulted in a strong reduction in mCherry-eEF1A fluorescence, whereas GFP was unaffected (Figure 1E). Loss of mCherry-eEF1A was dependent on the ternatin-4 concentration (EC$_{50}$ $\sim$5 nM; Figure S1B) and treatment time (t$_{1/2}$ $\sim$ 5 h; Figure S1C), and it was prevented by co-treatment with either a proteasome inhibitor or ribosome-targeted translation inhibitors (Figure S1D). Importantly, ternatin-4 had no effect on mCherry-eEF1A bearing the A399V mutation, which confirms that ternatin-4 binding is required to promote eEF1A degradation (Figure S1E).

We transduced the mCherry-eEF1A reporter cells with a focused sgRNA library targeting $\sim$1,700 genes primarily involved

in ubiquitin signaling and proteostasis (5 sgRNAs/gene; see Table S1 for the complete list of genes), plus 250 nontargeting sgRNAs.[30] Transduced cells were treated with ternatin-4 for 8 h or left untreated, followed by sorting into high and low fluorescence populations based on mCherry normalized to GFP (Figure 2A). For each population, sgRNA frequencies were quantified by Illumina sequencing and analyzed using our established bioinformatics pipeline.[31,32] We focused on genes whose knockdown led to increased mCherry-eEF1A levels (less degradation) in ternatin-treated but not untreated cells. Two E3 ligase genes, *RNF14* and *RNF25*, emerged as the most prominent hits (Figure 2B).

The knockdown of either RNF14 or RNF25 strongly prevented eEF1A degradation, with multiple sgRNAs enriched in the high mCherry-eEF1A population of ternatin-treated cells (Figure S2A). By contrast, sgRNAs targeting previously characterized ribosome-associated E3 ligases and RQC factors—including ZNF598, LTN1, RNF10, and CNOT4—had little or no effect on eEF1A degradation (Figure S2B; Table S1). To validate RNF14 and RNF25, we retested individual, top-scoring sgRNAs in our mCherry-eEF1A reporter cells and observed a complete loss of ternatin-induced degradation (Figure 2C).

RNF14 (also called ARA54)[33] belongs to the RING-between-RING (RBR) class of E3 ligases, which transfer ubiquitin from an E2 bound to the RING1 domain to a conserved catalytic cysteine (Cys417 in RNF14) in the RING2 domain.[34,35] By contrast, RNF25 (also called AO7)[36] is a RING-type E3 ligase. The deletion of RNF25 was recently found to sensitize cells to the alkylating agent methyl methanesulfonate (MMS) but not other DNA-damaging agents, indicating a potential role in repairing methylated DNA.[37] We note that MMS also methylates RNA and was found to activate the RQC pathway in yeast,[22] suggesting that MMS hypersensitivity of RNF25 KO cells could also stem from effects related to translation. Both RNF14 and RNF25 contain N-terminal RING finger and WD repeat-containing proteins and DEAD-like helicases (RWD) domains (Figure 2D), protein interaction domains found in $\sim$30 diverse human proteins exemplified by the ribosome-associated stress kinase, GCN2. Overall, the biological functions of RNF14 and RNF25 remain poorly understood.

To further validate RNF14 and RNF25, we generated HeLa knockout cell lines using CRISPR-Cas9. Similar to our CRISPRi knockdown results with mCherry-eEF1A, the knockout of either RNF14 or RNF25 abolished the ternatin-induced degradation of endogenous eEF1A while having no effect on eEF1A levels in untreated cells (Figure 2E). This phenotype was consistently observed across multiple RNF14 and RNF25 KO clones (Figure S2C). Concomitant with eEF1A degradation, the ternatin-4 treatment of wild-type (WT) HeLa cells caused a dramatic reduction in endogenous RNF14 levels. Remarkably, this effect was also abolished in RNF25 KO cells (Figure 2E). These results suggest that (1) RNF14, although an essential mediator of eEF1A

(C) CRISPRi reporter cells were transduced with the top-scoring *RNF14* and *RNF25* sgRNAs, treated with ternatin-4, and analyzed by flow cytometry.
(D) Domain organization of RNF14 and RNF25.
(E) RNF14 and RNF25 HeLa KO cells were generated using CRISPR-Cas9. Cells were then transduced with V5-tagged RNF14 or RNF25 constructs (containing IRES-mCherry) and sorted to produce pure populations. Cells were treated with ternatin-4 for 20 h and analyzed by immunoblotting.
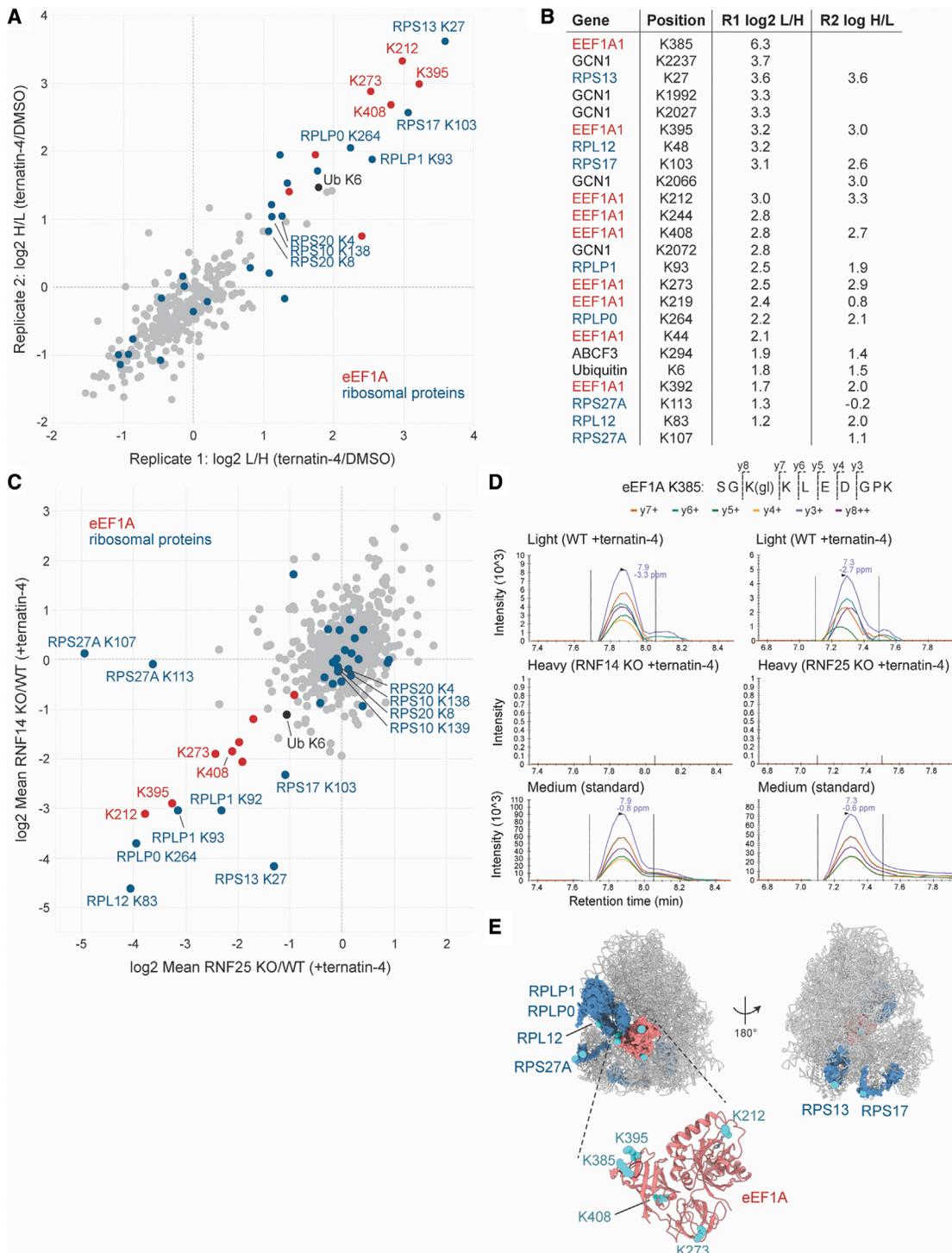See also Figure S2 and Table S1.

Figure 3. Ternatin-4 promotes RNF14 and RNF25-dependent ubiquitination of eEF1A and ribosomal proteins

(A) SILAC ratios (ternatin-4/DMSO) for diGly sites identified in two biological replicates from HeLa cells overexpressing RNF14 and treated ±ternatin-4 for 4 h.

(B) SILAC ratios for top-ranked diGly sites (eEF1A and ribosome-associated proteins) from each of the two biological replicates in (A).

(C) SILAC ratios (KO/WT) for diGly sites identified from WT and RNF14 or RNF25 KO cells treated with ternatin-4 for 4 h. Ratios are the average of two biological replicates (H/L label swaps).

(legend continued on next page)

destruction, is also degraded in response to ternatin-4 treatment and that (2) RNF25 plays an essential role in ternatin-induced degradation of both eEF1A and RNF14.

The reintroduction of WT RNF14 and RNF25 into their respective KO cells restored eEF1A degradation, confirming an essential role for both E3 ligases (Figure 2E). The overexpression of WT RNF14 rescued and further enhanced eEF1A degradation in the KO cells, whereas the overexpression of the catalytic Cys417 to Ala mutant failed to restore degradation. Likewise, the expression of WT RNF25, but not a RING deletion mutant, restored the degradation of both eEF1A and RNF14 in the RNF25 KO cells (Figure 2E). The overexpression of RNF14, but not RNF25, in WT cells also led to enhanced eEF1A degradation, whereas a catalytically dead mutant of RNF14 (but not RNF25) acted in a dominant negative manner, completely abrogating eEF1A degradation (Figure S2D). These results suggest that the ubiquitin ligase activity of RNF14 is rate limiting for eEF1A degradation and that overexpression of catalytically dead RNF14 can saturate a binding site required to promote eEF1A degradation.

RNF14 and RNF25 mediate the ubiquitination of eEF1A and ribosomal proteins

Having established the essential roles of RNF14 and RNF25 E3 ligase activity in eEF1A degradation, we sought to determine the global landscape of RNF14/RNF25-dependent ubiquitination sites in an unbiased manner. To do this, we used an established SILAC proteomics workflow in which tryptic peptides containing a ubiquitin-derived diGly remnant (attached to a substrate lysine residue) are immuno-enriched and quantified by mass spectrometry (MS).[38] We first treated cells stably overexpressing RNF14 with or without ternatin-4 for 4 h in two biological replicates (SILAC light/heavy label swaps; see STAR Methods). Cell lysates from each treatment condition (±ternatin-4) were combined and digested with trypsin, prior to the enrichment of diGly peptides (Figure S3A). MS analysis revealed >800 ubiquitination sites, 7 of which were strongly and reproducibly increased by ternatin-4 (log$_2$-fold change >2, Figure 3A). Strikingly, all 7 top-ranked sites were found either in eEF1A (4 sites) or the ribosomal proteins RPLP0, RPS13, and RPS17. Several ubiquitination sites in proteins relevant to translation elongation—including 7 additional eEF1A sites—were induced to a somewhat lower extent (log$_2$-fold change >1) or were identified in only one biological replicate (Figure 3B; Table S2), as is typical in data-dependent acquisition MS (DDA-MS). Of all identified ubiquitination sites, eEF1A K385 was induced most strongly by ternatin, increasing by at least 75-fold (Figures 3B and S3B). In addition, the ternatin-4 treatment led to the increased ubiquitination of multiple sites within the C-terminal region of the ribosome collision sensor, GCN1 (Figures 3B and S3B), as well as ABCF3 (ortholog of yeast Gcn20) and the ribosomal proteins, RPL12 and RPS27A (Figure 3B). K6-linked ubiquitin was elevated in the presence of ternatin-4 (Figures 3A and 3B), whereas other

ubiquitin linkage types were unaffected (Table S2). Although increased K6-linked polyubiquitination was previously observed in response to UV irradiation or p97/VCP inhibitors,[39,40] the specific functions of this linkage type remain poorly understood. We repeated the diGly SILAC-MS experiment (±ternatin-4) in RNF14-overexpressing cells co-treated with a proteasome inhibitor and in WT cells (without proteasome inhibitor treatment or RNF14 overexpression), and we observed similar levels of ternatin-induced eEF1A and ribosomal protein ubiquitination (Figures S3B and S3C; Table S2).

We next employed SILAC-MS to quantify ternatin-induced ubiquitination sites in RNF14 or RNF25 KO cells, relative to the parental WT cells. Consistent with their obligate roles in eEF1A degradation, the knockout of either RNF14 or RNF25 dramatically reduced eEF1A ubiquitination at multiple sites (Figure 3C; Table S2). The ubiquitination of a discrete set of ribosomal protein sites (including RPLP0 K264, RPLP1 K92, RPLP1 K93, and RPL12 K83), as well as K6-linked ubiquitin, was similarly reduced in both knockout cell lines. By striking contrast, the ubiquitination of RPS27A at K107 and K113 was reduced in RNF25 KO but not RNF14 KO cells, suggesting that these ubiquitination events are selectively mediated by RNF25 (Figure 3C). The ubiquitination of ZNF598-dependent sites on RPS10 and RPS20[12,41,42] was unaffected by either RNF14 or RNF25 knockout (Figure 3C; Table S2), despite increasing ~2-fold in response to ternatin-4 treatment (Figure 3B; Table S2). These data suggest that ternatin-induced stalls can activate distinct ribosome-associated ubiquitination events, which are mediated independently by ZNF598 and RNF14/RNF25.

Many of the ternatin-induced, RNF14/RNF25-dependent ubiquitination sites are also induced by UV irradiation, as revealed by a previously published dataset[39] (Figure S3D). We therefore performed a diGly SILAC-MS experiment comparing UV-irradiated RNF14 KO vs. rescue cells. UV-induced ubiquitination of eEF1A K392, ribosomal protein sites (e.g., RPLP1 K92/K93, RPLP0 K264, and RPL12 K48), and ubiquitin K6 was diminished in the absence of RNF14 (Figure S3E), whereas the ubiquitination of DNA damage response proteins (e.g., FANCI K523, XPC K174, and PCNA K164) was unaffected (Table S2). These data indicate that UV irradiation, an environmental stressor that induces ribosome collisions via photo-damaged mRNA,[21] can also activate the RNF14/RNF25 pathway.

The ubiquitination site most strongly induced by ternatin-4, eEF1A K385, was not identified in every biological replicate—this is likely due to the presence of a missed trypsin cleavage site after K386, as the fully trypsinized tetrapeptide would be too short to identify unambiguously. However, across multiple independent SILAC-MS experiments in which it was identified, K385 ubiquitination was consistently and dramatically induced by ternatin treatment, suggesting its likely dependence on RNF14/RNF25. To test this rigorously, we spiked in a synthetic "medium heavy" peptide standard (SGK[diGly]KLEDGPK, synthesized with heavy Leu), which facilitated the identification

(D) Samples from (C) were analyzed by PRM-MS for eEF1A K385 ubiquitination. Chromatograms are shown for one biological replicate (left: RNF14 KO vs. WT, right: RNF25 KO vs. WT). MS2 transitions were monitored for light (WT cells), heavy (KO cells), and medium (synthetic peptide standard) variants of SGK[diGly]KLEDGPK.
(E) Cartoon showing the location of ternatin-induced and RNF14/25-dependent ubiquitination sites (cyan spheres) on eEF1A and ribosomal proteins (PDB: 5LZS; RPLP0/RPLP1 based on PDB: 4V6X). The loop containing eEF1A K385 (residues 379–386) is colored in dark red.
See also Figure S3 and Table S2.

and quantification of the endogenous SILAC-derived peptides (SGK[diGly]KLEDGPK, containing 3 light or heavy Lys) via parallel reaction monitoring MS (PRM-MS) instead of DDA-MS (see STAR Methods for details). These experiments unambiguously revealed diGly-modified eEF1A K385 in ternatin-treated WT cells, whereas it was undetectable in either RNF14 or RNF25 knockout cells (Figure 3D).

We conclude that ternatin-induced elongation stalls promote the ubiquitination of multiple sites on eEF1A and a discrete set of ribosomal proteins. Most ternatin-induced ubiquitination sites are dependent on both RNF14 and RNF25, whereas RPS27A ubiquitination selectively requires RNF25. Several of the ribosomal ubiquitination sites we identified—including those on RPLP0, RPLP1, RPL12, and RPS27A—are proximal to the GTPase center where eEF1A binds, consistent with the notion that RNF14/RNF25-dependent eEF1A ubiquitination occurs on elongation-stalled ribosomes (Figure 3E). By contrast, RPS13 and RPS17 sites—which are also ternatin-induced and RNF14/RNF25-dependent—localize to a distinct region of the 40S subunit near the interface of collided di-ribosomes.

K385 is required for efficient eEF1A degradation and is directly ubiquitinated by RNF14

To assess the functional relevance of ternatin-induced, RNF14/RNF25-dependent eEF1A ubiquitination sites identified by MS, we introduced lysine to arginine mutations into the mCherry-eEF1A reporter. With the exception of K385, mutation of individual lysines had little or no effect on eEF1A degradation kinetics. By contrast, the ternatin-induced degradation of K385R eEF1A was impaired (Figures 4A and 4B). K385 resides on a flexible loop in the C-terminal beta-barrel domain of eEF1A (Figure 3E). This loop lies near the interface between the C-terminal domain and the N-terminal GTPase domain of ribosome-bound eEF1A and directly contacts the ternatin/didemnin binding site.[23,24] The mutagenesis results suggest that K385 ubiquitination, which is dramatically increased in the context of ternatin-induced stalls, plays a critical role in subsequent events leading to proteasome-dependent eEF1A degradation. Additional ternatin-induced ubiquitination sites, as revealed by our SILAC-MS experiments, may also contribute collectively to promoting efficient eEF1A degradation.

Based on the genetic evidence implicating RNF14 and RNF25 in ternatin-induced eEF1A ubiquitination and degradation, we hypothesized that one or both E3 ligases directly ubiquitinate eEF1A K385. To test whether this occurs in cells, we turned to a biotin-transfer assay in which an E3 of interest is fused to the biotin ligase BirA.[43–45] This proximity-based biotinylation assay relies on the specificity of BirA for an acceptor peptide fused to ubiquitin (AP-Ub). Expression of the BirA-E3 fusion protein results in the biotinylation of a proximal E2-bound AP-Ub, followed by the transfer of biotin-AP-Ub to an adjacent substrate (Figure 4C). The enrichment of biotinylated proteins with streptavidin-conjugated beads allows the detection of ubiquitinated substrates specific to the BirA-E3 ligase of interest.

We established the BirA-E3 proximity biotinylation assay in our ternatin-resistant HCT116 cell line (eEF1A1$^{A399V/A339V}$), modified to stably express FLAG-eEF1A. Strikingly, the treatment of cells co-expressing BirA-RNF14 and AP-Ub with ternatin-4 for 4 h re-

sulted in the specific enrichment of one major (mono-Ub) and two minor (di- and tri-Ub) higher-molecular weight forms of FLAG-eEF1A (Figures 4D and S4A). The transfer of biotin-AP-Ub to FLAG-eEF1A was not observed in cells expressing similar levels of BirA or an active site mutant of BirA-RNF14 (C417A), and it was barely detectable in cells expressing BirA-RNF25 (Figure 4D). Conversely, BirA-RNF25 (but not BirA-RNF14 or BirA-RNF25-dRING) promoted robust ubiquitination of RPS27A K113 (Figure S4B), consistent with the SILAC-MS data (Figure 3C). Finally, we observed a drastic decrease in BirA-RNF14-mediated ubiquitination of K385R FLAG-eEF1A (Figure 4E). These results suggest that RNF14 can directly promote eEF1A K385 ubiquitination in response to ternatin-induced elongation stalls. By contrast, the essential role of RNF25 in the eEF1A degradation pathway likely involves direct ubiquitination of RPS27A K113 (see below).

GCN1 interacts with RNF14 and is essential for eEF1A degradation

Besides eEF1A and ribosomal proteins, our diGly proteomics experiments revealed multiple ternatin-induced ubiquitination sites on GCN1. GCN1 is a conserved ribosome-associated scaffolding protein that binds the RWD domain of the integrated stress response kinase, GCN2.[46,47] In addition, GCN1 was recently shown to interact with collided, elongation-stalled ribosomes in yeast[20] and human cells,[21] although the relative binding affinities of GCN1 for monosomes vs. disomes, trisomes, etc. remain unknown. We postulated that GCN1 (which was not included in the CRISPRi screen) might play a direct role in RNF14/RNF25-mediated eEF1A degradation.

To evaluate potential interactions with GCN1, we immunoprecipitated FLAG-tagged RNF14 or RNF25 (stably expressed in HeLa cells). Because previous studies employed chemical crosslinking to stabilize protein interactions with GCN1,[21,48] we briefly treated cells with 0.1% formaldehyde (22C, 10 min) prior to preparing detergent lysates for immunoprecipitation. This experiment revealed a specific interaction between FLAG-RNF14 and endogenous GCN1 in cells treated with or without ternatin (Figure 5A). A higher-molecular weight, likely multi-ubiquitinated form of GCN1 was specifically enriched in FLAG-RNF14 immunoprecipitates from ternatin-treated cells, whereas this higher-molecular weight GCN1 species was not detected in immunoprecipitates from untreated cells or from ternatin-treated cells expressing a catalytically dead mutant (C417A) of FLAG-RNF14 (Figures 5A and S5A). Multi-ubiquitinated GCN1 bound to FLAG-RNF14 was observed in cells treated for 1 h with intermediate but not high concentrations of ternatin-4 (Figure S5B), providing additional evidence that RNF14 is activated by ribosome collisions. Relative to FLAG-RNF14, FLAG-RNF25 enriched GCN1 to a lesser extent, yet robustly immunoprecipitated endogenous 40S and 60S ribosomal proteins, even in the absence of chemical crosslinking (Figure 5A). These results suggest that RNF14 and RNF25 can form complexes containing GCN1 and ribosomes, consistent with a requirement for both E3 ligases in ternatin-induced ubiquitination of eEF1A and ribosomal proteins (Figure 3) and the established role of GCN1 as a sensor for elongation-stalled ribosomes.[20–22,49] The data also suggest that RNF14 may directly ubiquitinate GCN1 in response
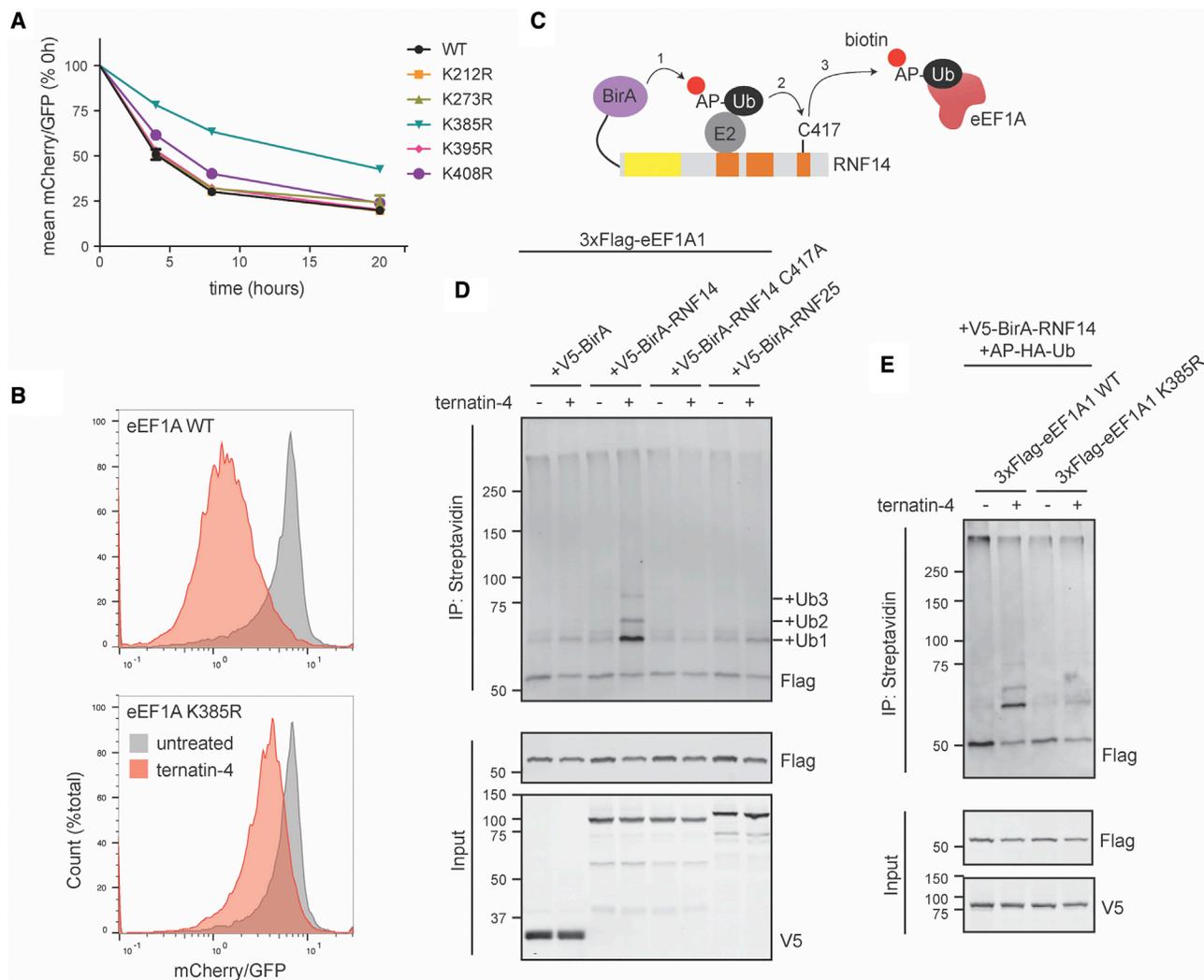
Figure 4. eEF1A K385 is required for efficient degradation and is directly ubiquitinated by RNF14

(A) Ternatin-resistant HCT116 cells expressing WT and Lys mutant mCherry-eEF1A reporter constructs were treated with ternatin-4 and analyzed by flow cytometry. Plotted are the mean mCherry/GFP ratios (n = 3, ±SEM) relative to t = 0 h for each mutant.

(B) Histograms for cells from (A) expressing WT or K385R eEF1A and treated ±ternatin-4 for 8 h.

(C) Schematic for proximity-based biotin-transfer assay. Acceptor peptide (AP)-ubiquitin is biotinylated when bound to E2 and the biotin ligase BirA-RNF14 fusion. Biotinylated AP-Ub is subsequently transferred to E3 substrates, which are enriched via streptavidin.

(D) Ternatin-4 induces proximity-mediated eEF1A ubiquitination by RNF14 but not RNF25. Ternatin-resistant HCT116 cells stably expressing 3xFLAG-eEF1A1 were co-transfected with AP-HA-Ub and the indicated BirA fusion constructs. Cells were treated with 50 μM biotin ± ternatin-4 for 4 h.

(E) As in (D), except with cells expressing WT or K385R 3xFLAG-eEF1A.

See also Figure S4.

to ternatin-induced stalls, although the functional relevance of these marks is unclear.

GCN1-interacting proteins other than GCN2 remain relatively unexplored in higher eukaryotes. By contrast, a conserved C-terminal region of yeast Gcn1, which includes R2259, has been shown to mediate interactions with the RWD domains of yeast Gcn2, Yih1, and Gir2.[20,50] Mutation of Gcn1 R2259 (corresponding to R2312 in human GCN1) had no effect on binding to ribosomes or Gcn20, yet abolished interactions with Gcn2 and prevented Gcn2 activation upon amino acid starvation.[46] Like GCN2, both RNF14 and RNF25 contain RWD domains, which

we hypothesized could mediate interactions with the conserved GCN2-binding region of GCN1. Consistent with the above results using overexpressed RNF14/RNF25 (Figure 5A), reciprocal immunoprecipitation of overexpressed GCN1-FLAG confirmed binding to endogenous RNF14, whereas binding to endogenous RNF25 could not be reliably detected over background (Figure 5B). Importantly, the mutation of R2312 in the conserved RWD-binding region of GCN1 dramatically reduced interaction with RNF14 but not ribosomal proteins. GCN2 binding was likewise diminished with GCN1 R2312A, although to a lesser extent than RNF14.
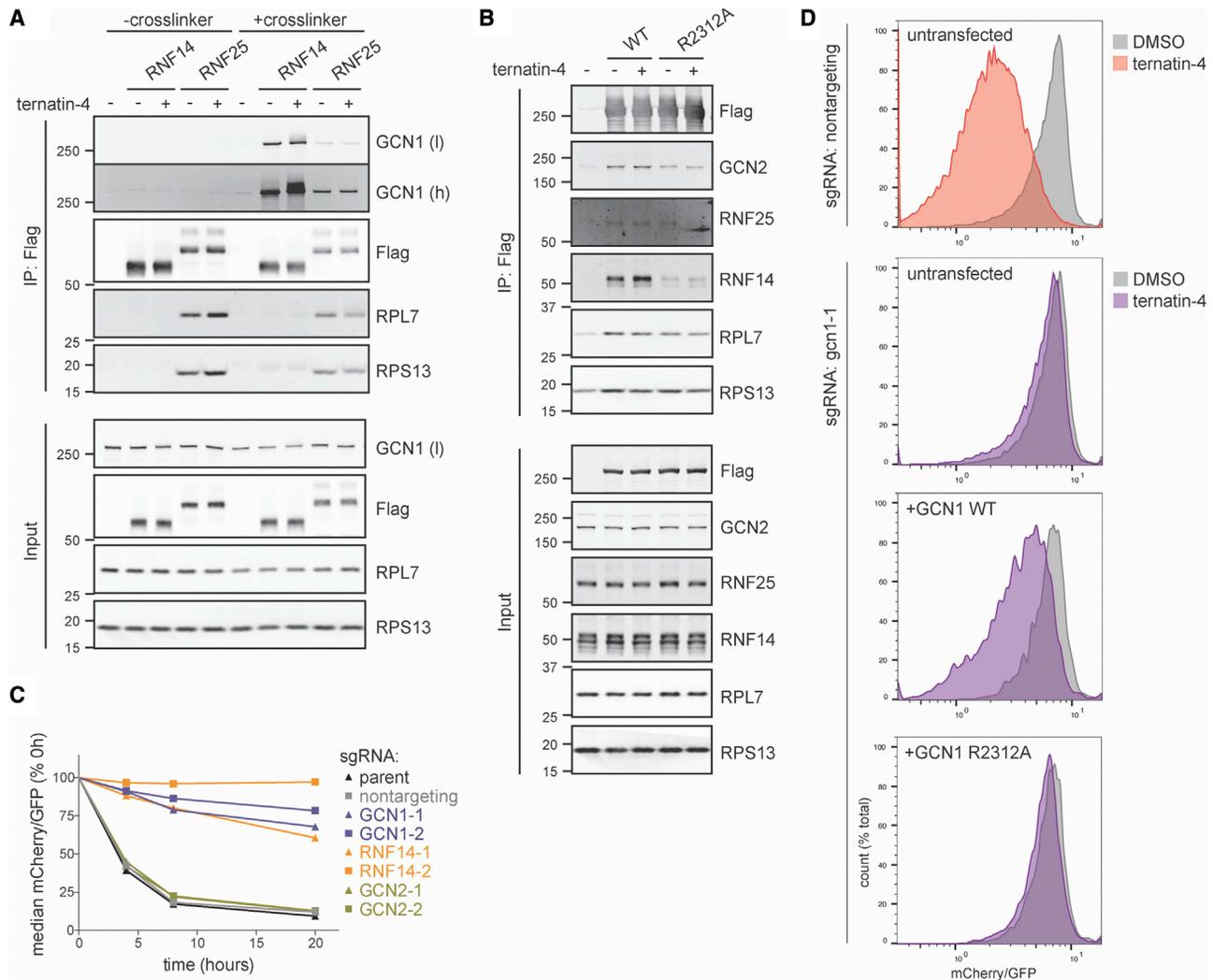
⬦ CellPress

Figure 5. GCN1 interacts with RNF14 and is essential for eEF1A degradation

(A) HeLa cells stably expressing 3xFLAG-tagged RNF14 or RNF25 were treated ±ternatin-4 for 4 h and then crosslinked with 0.1% PFA (10 min, 22°C) prior to cell lysis, FLAG immunoprecipitation, and immunoblotting.

(B) HEK293T cells transfected with WT or R2312A GCN1-3xFLAG were treated and analyzed as in (A).

(C) CRISPRi mCherry-eEF1A reporter cells were transduced with the indicated sgRNAs, treated with ternatin-4, and analyzed by flow cytometry.

(D) CRISPRi reporter cells were transduced with nontargeting or GCN1-targeted sgRNAs and subsequently transfected with WT or R2312A GCN1-3xFLAG. Cells were treated ±ternatin-4 for 8 h and analyzed by flow cytometry.

See also Figure S5.

To test for a functional role of GCN1 in eEF1A degradation, we used CRISPRi and the mCherry-eEF1A reporter assay. Remarkably, GCN1 knockdown diminished ternatin-induced eEF1A degradation to a similar extent as RNF14 knockdown (Figures 5C and S5C), whereas the knockdown of the canonical GCN1 partner, GCN2, had no effect. Impaired eEF1A degradation was partially rescued in the CRISPRi knockdown cells upon the overexpression of WT GCN1. By contrast, the RNF14 binding-defective GCN1 mutant (R2312A) completely failed to restore eEF1A degradation in cells depleted of endogenous GCN1 (Figures 5D and S5D). Collectively, the results in Figure 5 demonstrate that GCN1, which has previously been linked to the activation of the integrated stress response kinase GCN2,

forms a distinct functionally relevant complex with the E3 ligase RNF14.

RNF25-dependent ubiquitination of RPS27A K113 is essential for eEF1A degradation

The mechanistic experiments presented above support a specific role for RNF14, which forms a complex with GCN1 and directly ubiquitinates eEF1A, but they do not account for the essential role of RNF25 in the pathway. Our diGly proteomics data provided a potential clue to this puzzle, which was further corroborated by the BirA-RNF25 assay (Figure S4B). The ubiquitination of RPS27A (aka eS31) at K107 and K113 was found to be uniquely dependent on RNF25 and not RNF14, whereas the
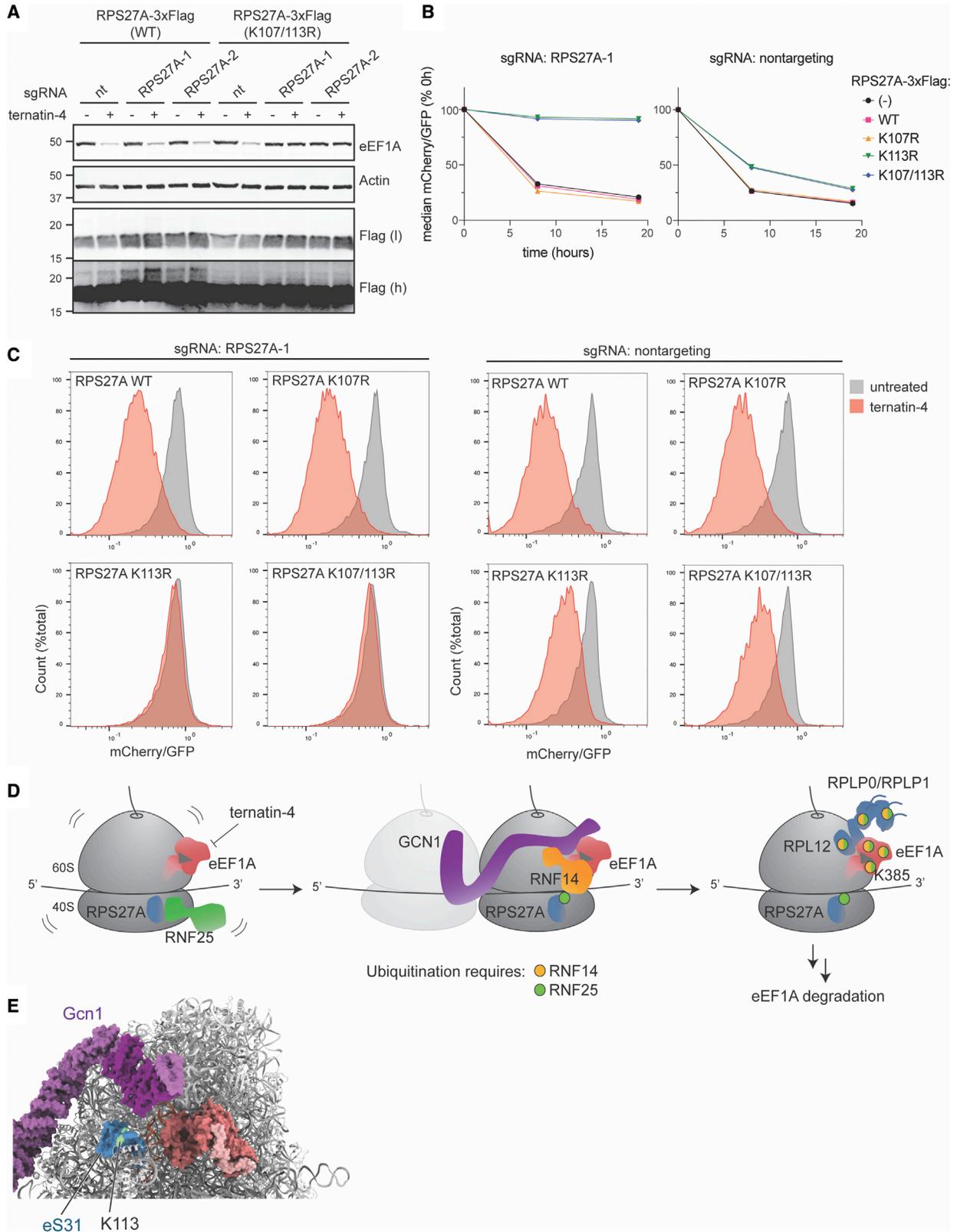
(legend on next page)

ubiquitination of eEF1A and other ribosomal proteins required both RNF25 and RNF14 (Figure 3C). These data are consistent with an E3 signaling cascade: RNF25 directly promotes RPS27A ubiquitination, which is essential for subsequent RNF14-mediated ubiquitination events on stalled ribosomes. To test whether RPS27A ubiquitination is required for eEF1A degradation, we employed a CRISPRi-mediated knockdown and rescue strategy. HeLa CRISPRi cells (stably expressing dCas9-BFP-KRAB) were first transduced with lentiviral constructs encoding either WT or K107/113R mutant RPS27A-FLAG. The resulting cell lines, which stably express exogenous RPS27A, were next transduced with sgRNAs to selectively knock down endogenous RPS27A (Figure S6A). Upon treatment with ternatin-4, we observed robust eEF1A degradation in cells expressing WT RPS27A-FLAG (Figure 6A). By contrast, eEF1A degradation was abolished in RPS27A knockdown cells expressing the K107/113R mutant, strongly supporting a role for the RNF25-dependent ubiquitination of K107 and/or K113. Immunoblot analysis of the cells expressing WT RPS27A-FLAG, but not the K107/113R mutant, revealed low levels of a higher-molecular weight band consistent with mono-ubiquitination of K107 and/or K113.

We confirmed and extended these results by monitoring mCherry-eEF1A degradation in the HCT116 CRISPRi cells, which were engineered to stably express the following RPS27A-FLAG constructs: WT, K107R, K113R, or K107/113R. Strikingly, mCherry-eEF1A degradation was completely prevented in ternatin-treated cells expressing K113R RPS27A-FLAG (or the K107/113R double mutant) and transduced with an sgRNA targeting endogenous RPS27A (Figures 6B and 6C). By contrast, the K107R single mutant was indistinguishable from WT RPS27A-FLAG and supported the robust degradation of mCherry-eEF1A. Even without the sgRNA-mediated knockdown of endogenous RPS27A, the expression of exogenous K113R or K107/113R RPS27A-FLAG partially reduced mCherry-eEF1A degradation (Figures 6B and 6C).

The stable overexpression of RNF25 (but not RNF14) in HeLa cells resulted in increased levels of mono-ubiquitinated WT (but not K113R) RPS27A-FLAG (Figure S6B), facilitating its analysis by sucrose density gradient centrifugation. Using these cells, we confirmed that ubiquitinated and unmodified RPS27A-FLAG cofractionate with 80S monosomes and polysomes, indicating that both forms of RPS27A-FLAG are constituents of actively trans-

lating ribosomes (Figure S6C). Upon the treatment of cell lysates with micrococcal nuclease, RPS27A-FLAG predominantly cofractionated with 80S monosomes; however, both ubiquitinated and unmodified forms were also detected in fractions containing nuclease-resistant disomes and in ternatin-treated cells, trisomes (Figure S6D). Collectively, our RPS27A knockdown/rescue experiments strongly suggest that the direct RNF25-dependent ubiquitination of RPS27A on K113 plays an essential upstream role in the E3 signaling cascade, ultimately promoting RNF14-dependent eEF1A ubiquitination and degradation on stalled ribosomes (Figure 6D). A recent cryo-EM structure of yeast Gcn1 bound to a stalled ribosome reveals that RPS27A K113 lies in close proximity to the RWD-binding domain of Gcn1, as well as the ribosomal A site (Figure 6E), suggesting that K113-Ub could potentially activate GCN1-bound RNF14 (see discussion).

RNF14 and RNF25 promote the degradation of the termination factor eRF1

Our findings with ternatin-4 and eEF1A raise a key question: does the RNF14/RNF25 pathway monitor other translation factors (including termination factors) that may become stalled in the ribosomal A site? A synthetic small molecule, SRI-41315, was recently shown to induce the degradation of the termination factor eRF1 (but not its binding partner, the GTPase eRF3) by an unknown mechanism, resulting in enhanced stop codon readthrough.[51] We hypothesized that SRI-41315 might impair eRF1 functions during translation termination and thus activate the RNF14/RNF25 pathway. Consistent with the previous report,[51] the treatment of HeLa cells with SRI-41315 for 20 h resulted in a dramatic loss of eRF1. Strikingly, eRF1 degradation was completely prevented in RNF14 KO or RNF25 KO cells and rescued by the reintroduction of the corresponding E3 ligase into KO cells (Figure 7A). Simultaneous treatment with SRI-41315 and either CHX or HHT also prevented eRF1 degradation (Figure 7B), demonstrating a requirement for active translation.

Acute treatment of RNF14 rescue cells with SRI-41315 for 1 h decreased total eRF1 levels by >50% and resulted in the formation of higher-molecular weight, presumably ubiquitinated eRF1 species (Figure 7C, input), an effect that was not observed in RNF14 KO cells (Figure S7A). Consistent with eRF1 ubiquitination, affinity enrichment using an affimer specific for K6-linked ubiquitin chains[52] revealed a dramatic increase in K6-ubiquitinated eRF1 (but not eEF1A) in cells treated with SRI-41315 but

---

Figure 6. Ubiquitination of RPS27A/eS31 K113 is essential for eEF1A degradation

(A) HeLa CRISPRi cells stably expressing WT or K107/113R RPS27A-3xFLAG were transduced with nontargeting or endogenous RPS27A-targeting sgRNAs. sgRNA-expressing cells were treated ±ternatin-4 for 20 h.

(B) mCherry-eEF1A/CRISPRi reporter cells (Figure 1E) were first transduced with RPS27A-3xFLAG constructs and then sgRNAs as in (A). Cells were treated with ternatin-4 and analyzed by flow cytometry.

(C) Flow cytometry histograms from cells in (B) treated ±ternatin-4 for 8 h.

(D) Model for GCN1/RNF14/RNF25 surveillance pathway. RNF25 binds translating ribosomes in unstressed cells and ubiquitinates RPS27A K113 in response to transient stalling events. Upon ternatin-induced stalling, GCN1-bound RNF14 is recruited to ribosome collisions, leading to ubiquitination of trapped eEF1A and the adjacent ribosomal proteins RPL12, RPLP0, and RPLP1. The ubiquitination of eEF1A K385 and other sites leads to proteasome-dependent eEF1A degradation.

(E) Cryo-EM-derived model of yeast Gcn1/di-ribosome complex (PDB: 7NRC) showing Gcn1 (purple) bound to the leading (stalled) ribosome. The C-terminal RWD-binding region of Gcn1 (bright purple) is proximal to K113 (green) of eS31 (blue; yeast ortholog of human RPS27A/eS31) and the GTPase center, which in this structure contains the yeast Gir2/Rbg2 complex (pink/red) bound to peptidyl-tRNA in the A site. Maximal RNF14 E3 ligase activity may require interactions with GCN1 and ubiquitinated RPS27A/eS31 K113.
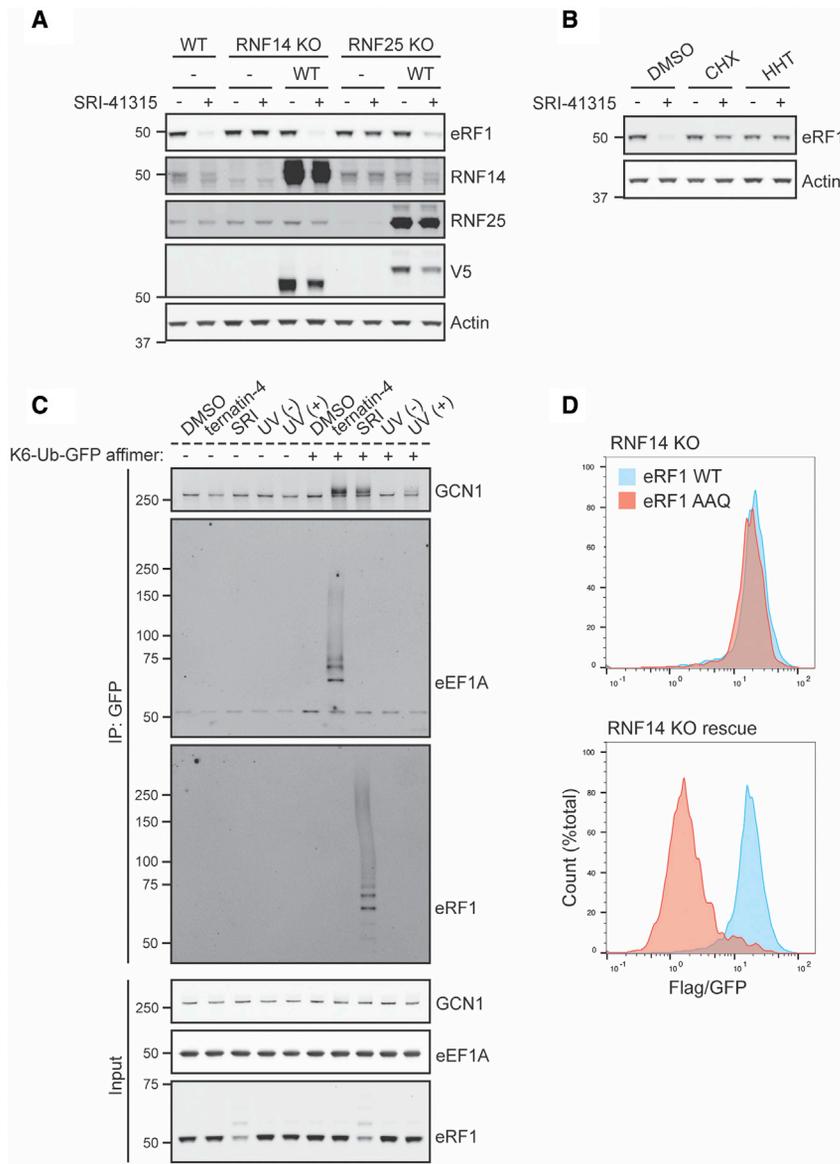
See also Figure S6.

Figure 7. RNF14 and RNF25 promote degradation of the termination factor eRF1

(A) HeLa WT, KO, or rescue cells (Figure 2E) were treated ±10 μM SRI-41315 for 20 h, and eRF1 levels were analyzed.

(B) HeLa WT cells were treated with SRI-41315 in the presence or absence of CHX or HHT for 20 h.

(C) HeLa RNF14 KO rescue cells were treated with DMSO, ternatin-4, or SRI-41315 for 1 h, or were irradiated with 40 J/m^2 UV (or no-UV control) and allowed to recover for 1 h. Cell lysates were incubated with or without a GFP-conjugated affimer for K6-linked ubiquitin, and bound species were enriched using a GFP nanobody.

(D) HeLa RNF14 KO or rescue cells were transduced with constructs containing WT or AAQ mutant 3xFLAG-eRF1 and IRES-GFP. Cells were fixed, permeabilized, stained with anti-FLAG-allophycocyanin (APC), and analyzed by flow cytometry. GFP-positive cells are displayed in histograms.

See also Figure S7.

To test directly whether impaired eRF1 activity is sufficient to promote RNF14-dependent degradation, we took advantage of a catalytically inactive eRF1 variant in which the conserved GGQ motif is mutated to AAQ (G183/184A). Such eRF1 mutants can recognize stop codons in the A site,[24,53] but they fail to catalyze peptidyl-tRNA hydrolysis, thus promoting ribosome collisions.[12,22] RNF14 KO or rescue cells were stably transduced with FLAG-tagged WT or mutant eRF1 linked to an IRES-GFP and analyzed by flow cytometry. In RNF14 rescue cells, steady-state levels of FLAG-eRF1-AAQ were drastically reduced compared with WT FLAG-eRF1 (Figures 7D and S7B). By contrast, there was no apparent difference between WT and mutant eRF1 levels in RNF14 KO cells. Similar results were obtained by immunoblotting for WT and mutant FLAG-eRF1 (Figure S7C). Collectively, our data suggest that the RNF14/RNF25 pathway can monitor the ribosomal A site during translation termination, promoting K6-linked polyubiquitination and degradation of stalled eRF1.

not ternatin-4 (Figure 7C). Conversely, K6-ubiquitinated eEF1A was enriched from cells treated with ternatin-4 but not SRI-41315. Finally, K6-ubiquitinated GCN1 was also dramatically increased in cells treated with ternatin-4 or SRI-41315. Affimer enrichment after UV irradiation revealed a modest increase in K6-ubiquitinated GCN1 but not eRF1 or eEF1A (Figure 7C), presumably reflecting the weaker activation of the RNF14/RNF25 pathway by UV-damaged RNA. Notably, the observed increase in K6-ubiquitinated eRF1, eEF1A, and GCN1 was prevented in cells lacking RNF14 (Figure S7A), consistent with our diGly SILAC-MS data showing decreased total K6-Ub in RNF14 KO cells (Figures 3C and S3E). Although its precise molecular mechanism remains to be elucidated, we speculate that SRI-41315 alters the conformation or dynamics of eRF1 within the ribosomal A site, resulting in RNF14/RNF25-dependent ubiquitination and degradation.

DISCUSSION

In this study, we investigated the cellular response to elongation stalls induced by ternatin-4, which traps eEF1A on the ribosome and prevents aa-tRNA accommodation.[25] We discovered that ternatin-4 robustly induces eEF1A degradation, and we used this phenotype as a foothold to elucidate a signaling pathway requiring two poorly characterized E3 ligases, RNF14 and RNF25. RNF14 and RNF25 act in concert with the ribosome collision sensor GCN1—best known as an upstream activator of the integrated stress response kinase

GCN2—to promote the ubiquitination and proteasome-dependent degradation of eEF1A.

Integrating our data with recently published work, we propose a detailed model for eEF1A ubiquitination on stalled ribosomes (Figure 6D). Because a fraction of RNF25 interacts with ribosomes even in unstressed cells, it may play an essential upstream surveillance role by promoting RPS27A K113 ubiquitination in response to pausing or stalling events. Consistent with this idea, we detected RPS27A K113 ubiquitination in untreated cells, which subsequently increased ~2-fold after treatment with ternatin-4 (Figures S3B and S3C; Table S2). Of note, the ubiquitination of RPS27A K113 was uniquely and solely dependent on RNF25 (and not RNF14), and the expression of K113R RPS27A in cells depleted of endogenous RPS27A abolished ternatin-induced eEF1A degradation. This represents one of only a few reported examples of functionally characterized ribosome ubiquitination sites in human cells.[13,41,54,55] Elevated RPS27A K113 ubiquitination requiring active translation has previously been observed in cells lacking the deubiquitinase USP16[56] or treated with low-dose emetine.[57] Although the relevant E3 ligase was not identified in either study, our results reveal RNF25 as a strong candidate. We propose that RNF25, likely via direct ubiquitination of RPS27A K113 (Figure S4B), provides one of two signaling inputs required to activate the RBR-type E3 ligase, RNF14: a potential mechanism for this requirement is described below.

GCN1 provides a second essential signaling input, most likely by recruiting and activating RNF14 near the occluded A site of stalled ribosomes. The cryo-EM structure of yeast Gcn1 bound to collided di-ribosomes suggests a potential mechanism,[20] as the RWD-binding domain of Gcn1 is positioned adjacent to the A site of the leading (stalled) ribosome (Figure 6E). Hence, the binding of this highly conserved region to the N-terminal RWD domain of RNF14 could facilitate proximity-based ubiquitination of eEF1A or eRF1 trapped on the ribosome, as well as GCN1 itself (all identified GCN1 Ub sites map to the C-terminal region) and the ribosomal proteins RPL12, RPLP0, and RPLP1. Although further studies are required to define the functions of these additional ubiquitin marks, we provide evidence here for direct RNF14-mediated ubiquitination of eEF1A K385, which is essential for maximal eEF1A degradation.

The yeast Gcn1/di-ribosome cryo-EM structure also provides clues to a potential role for the RNF25-dependent ubiquitination of RPS27A/eS31 K113. This ubiquitination site resides at the tip of the small ribosomal subunit "beak" and is immediately adjacent to the RWD-binding domain of Gcn1 (Figure 6E). This arrangement suggests a mechanism whereby RNF14 could receive two proximal signaling inputs: one provided by GCN1 binding to the RNF14 RWD domain, and a second provided by mono-ubiquitinated K113 on RPS27A. K113-Ub could potentially engage a conserved allosteric ubiquitin-binding site in the RBR domain of RNF14. Although speculative, this model is consistent with structural and biochemical studies of other RBR-type E3 ligases (e.g., parkin and HOIP), which are autoinhibited and require allosteric activation—including by ubiquitin itself—to unveil the E2 binding and catalytic sites.[58]

Historically, natural products with distinct proteotoxic mechanisms have been used to elucidate cellular stress response pathways, including the unfolded protein response (UPR) (tunicamycin), mitochondrial UPR (antimycin), and ribotoxic stress response (anisomycin). A strength of our study is the use of ternatin-4 to acutely induce ribosome stalls with trapped eEF1A, providing a robust elongation stress signal that culminates in ubiquitin-dependent eEF1A degradation. A key question for the future concerns the physiological and environmental stressors that activate the GCN1/RNF14/RNF25 pathway in cells and organisms. One potential environmental stressor is RNA-damaging UV light,[21,39] which promotes RNF14-dependent ubiquitination of eEF1A, several ribosomal proteins, and GCN1 (Figures 7C and S3E).

In addition to RNA damage, altered post-transcriptional RNA modifications—in particular, decreased methoxycarbonylmethylation or thiolation of the anticodon wobble uridine (U_{34}) in certain tRNAs—could result in codon-specific stalls that locally activate GCN1/RNF14/RNF25. Preliminary support for this idea is provided by a recent study that correlated genome-wide CRISPR knockout effects (https://depmap.org) across 485 cancer cell lines.[59] Based on a statistical analysis of gene-gene correlations ("co-essentiality"), RNF25 was placed in the same biological pathway as ELP3 and CTU2. The latter enzymes promote tRNA U_{34} methoxycarbonylmethylation and thiolation, respectively, and control translation elongation in developmental, homeostatic, and disease contexts.[60,61] Finally, ribosome stalling at termination codons could also activate the GCN1/RNF14/RNF25 pathway, leading to ubiquitination of eEF1A (bound to near-cognate aa-tRNA) or release factors (eRF1/eRF3) trapped in the GTPase center. Although overexpression of the RNF14 ortholog Itt1 was found to promote stop codon readthrough in yeast,[62] the mechanism underlying this phenotype was unclear. In this study, we demonstrate that RNF14 and RNF25 promote the degradation of a catalytically dead eRF1 mutant that stalls termination while trapped in the A site.[22,24,53] We further show that SRI-41315, a small molecule that was recently found to promote eRF1 degradation,[51] does so in a manner that critically requires RNF14 and RNF25.

The deletion of GCN1, or even the C-terminal RWD-binding region of GCN1, is lethal in mice,[63] whereas the deletion of GCN2 causes only mild phenotypes.[64] Hence, GCN1 must have GCN2-independent functions, which have remained enigmatic despite the identification of other RWD domain-containing Gcn1 interactors, including yeast Gir2 and Yih1.[20,65,66] Integrating results from our study with previous work, we propose that GCN1 lies at the nexus of multiple translation stress and surveillance pathways requiring RWD domain effectors—including RNF14 and RNF25—in which pathway selection is determined locally by the status and occupancy of the GTPase center and A site of the stalled ribosome.

Limitations of the study

A detailed mechanistic understanding of how RNF14 and RNF25 cooperate with GCN1 to promote ubiquitination of stalled eEF1A/ribosome complexes will require biochemical reconstitution from purified components, along with structural analysis of key intermediates. Such studies will be crucial for elucidating the

biochemical mechanisms by which RNF14 is recruited and activated, including the roles played by the RWD domains of RNF25 and RNF14, the RWD-binding domain of GCN1, and the K113-Ub mark on RPS27A/eS31. Further mechanistic insights will be gained by assessing the functions of additional RNF14/RNF25-dependent ubiquitination sites, including sites on GCN1, RPL12, RPLP0/P1, and RPS13. Although we demonstrate the activation of the RNF14/RNF25 pathway by multiple stressors (ternatin-4, UV light, and SRI-41315), leading to the degradation of distinct translation factors bound to the A site (eEF1A and eRF1), the physiological mediators of elongation and termination stalling that activate the pathway remain to be elucidated. Investigating the effects of RNF14/RNF25 deletion, mutation, and overexpression in developmental or disease contexts will provide insights into the physiological roles of this pathway. Although we employ ternatin-4 at concentrations that maximally promote eEF1A degradation, the extent to which rare physiological stalls activate the pathway is unclear—such stalling events likely result in decreased levels of eEF1A degradation. Finally, the crosstalk between the GCN1/RNF14/RNF25 pathway and other translation surveillance pathways (ribotoxic stress response, integrated stress response, and RQC) remains an important area for future investigation.

STAR★METHODS

Detailed methods are provided in the online version of this paper and include the following:

- KEY RESOURCES TABLE
- RESOURCE AVAILABILITY
  - Lead contact
  - Materials availability
  - Data and code availability
- EXPERIMENTAL MODEL AND SUBJECT DETAILS
  - Cell lines and culture conditions
- METHOD DETAILS
  - Plasmid Generation
  - Lentivirus and stable cell line generation
  - CRISPR knockout cell lines
  - Immunoblot analysis
  - Protein synthesis measurements
  - Flag-APC cell staining
  - Flow cytometry
  - CRISPRi screen
  - Individual sgRNA knockdown and rescue
  - RT-qPCR
  - DiGly peptide enrichment
  - LC-MS/MS data acquisition (DDA)
  - PRM analysis of eEF1A K385 ubiquitination
  - Proximity-based ubiquitination assay
  - K6-linked ubiquitin enrichment
  - Co-immunoprecipitations
  - Sucrose density gradient ultracentrifugation
- QUANTIFICATION AND STATISTICAL ANALYSIS
  - Quantification and normalization
  - CRISPRi screen analysis
  - Mass spectrometric site identification and quantification

AUTHOR CONTRIBUTIONS

K.O. designed and performed experiments and analyzed and interpreted data. J.D.C. designed experiments and developed the fluorescent reporter assay. S.K.S. assisted with planning and performing the CRISRPi screen and analyzed screen data. T.Y. collected MS data and assisted with MS data analysis. H.-Y.W. synthesized key reagents. M.K. assisted with planning the CRISPRi screen and interpreted data. J.T. supervised the study. J.D.C., K.O., and J.T. conceived the study. J.T. and K.O. wrote the manuscript with input from all authors.

REFERENCES

1. Dever, T.E., and Green, R. (2012). The elongation, termination, and recycling phases of translation in eukaryotes. Cold Spring Harb. Perspect. Biol. 4, a013706. https://doi.org/10.1101/cshperspect.a013706.

2. Sonenberg, N., and Hinnebusch, A.G. (2009). Regulation of translation initiation in eukaryotes: mechanisms and biological targets. Cell 136, 731–745. https://doi.org/10.1016/j.cell.2009.01.042.

3. Jackson, R.J., Hellen, C.U.T., and Pestova, T.V. (2010). The mechanism of eukaryotic translation initiation and principles of its regulation. Nat. Rev. Mol. Cell Biol. 11, 113–127. https://doi.org/10.1038/nrm2838.

4. Richter, J.D., and Coller, J. (2015). Pausing on polyribosomes: make way for elongation in translational control. Cell 163, 292–300. https://doi.org/10.1016/j.cell.2015.09.041.

5. Schuller, A.P., and Green, R. (2018). Roadblocks and resolutions in eukaryotic translation. Nat. Rev. Mol. Cell Biol. 19, 526–541. https://doi.org/10.1038/s41580-018-0011-4.

6. Stein, K.C., and Frydman, J. (2019). The stop-and-go traffic regulating protein biogenesis: how translation kinetics controls proteostasis. J. Biol. Chem. 294, 2076–2084. https://doi.org/10.1074/jbc.REV118.002814.

Cell
Article

CellPress

7. Brandman, O., and Hegde, R.S. (2016). Ribosome-associated protein quality control. Nat. Struct. Mol. Biol. *23*, 7–15. https://doi.org/10.1038/nsmb.3147.

8. Yip, M.C.J., and Shao, S. (2021). Detecting and rescuing stalled ribosomes. Trends Biochem. Sci. *46*, 731–743. https://doi.org/10.1016/j.tibs.2021.03.008.

9. Doma, M.K., and Parker, R. (2006). Endonucleolytic cleavage of eukaryotic mRNAs with stalls in translation elongation. Nature *440*, 561–564. https://doi.org/10.1038/nature04530.

10. Shoemaker, C.J., Eyler, D.E., and Green, R. (2010). Dom34:Hbs1 promotes subunit dissociation and peptidyl-tRNA drop-off to initiate no-go decay. Science *330*, 369–372. https://doi.org/10.1126/science.1192430.

11. Juszkiewicz, S., Speldewinde, S.H., Wan, L., Svejstrup, J.Q., and Hegde, R.S. (2020). The ASC-1 complex disassembles collided ribosomes. Mol. Cell *79*, 603–614.e8. https://doi.org/10.1016/j.molcel.2020.06.006.

12. Juszkiewicz, S., Chandrasekaran, V., Lin, Z., Kraatz, S., Ramakrishnan, V., and Hegde, R.S. (2018). ZNF598 is a quality control sensor of collided ribosomes. Mol. Cell *72*, 469–481.e7. https://doi.org/10.1016/j.molcel.2018.08.037.

13. Juszkiewicz, S., and Hegde, R.S. (2017). Initiation of quality control during poly(A) translation requires site-specific ribosome ubiquitination. Mol. Cell *65*, 743–750.e4. https://doi.org/10.1016/j.molcel.2016.11.039.

14. Matsuo, Y., Tesina, P., Nakajima, S., Mizuno, M., Endo, A., Buschauer, R., Cheng, J., Shounai, O., Ikeuchi, K., Saeki, Y., et al. (2020). RQT complex dissociates ribosomes collided on endogenous RQC substrate SDD1. Nat. Struct. Mol. Biol. *27*, 323–332. https://doi.org/10.1038/s41594-020-0393-9.

15. Matsuo, Y., Ikeuchi, K., Saeki, Y., Iwasaki, S., Schmidt, C., Udagawa, T., Sato, F., Tsuchiya, H., Becker, T., Tanaka, K., et al. (2017). Ubiquitination of stalled ribosome triggers ribosome-associated quality control. Nat. Commun. *8*, 159. https://doi.org/10.1038/s41467-017-00188-1.

16. Simms, C.L., Yan, L.L., Zaher, H.S., Simms, C.L., Yan, L.L., and Zaher, H.S. (2017). Ribosome collision is critical for quality control during no-go decay. Mol. Cell *68*, 1–13. https://doi.org/10.1016/j.molcel.2017.08.019.

17. Ikeuchi, K., Tesina, P., Matsuo, Y., Sugiyama, T., Cheng, J., Saeki, Y., Tanaka, K., Becker, T., Beckmann, R., and Inada, T. (2019). Collided ribosomes form a unique structural interface to induce Hel2-driven quality control pathways. EMBO J. *38*, e100276. https://doi.org/10.15252/embj.2018100276.

18. Meydan, S., and Guydosh, N.R. (2021). A cellular handbook for collided ribosomes: surveillance pathways and collision types. Curr. Genet. *67*, 19–26. https://doi.org/10.1007/s00294-020-01111-w.

19. Kim, K.Q., and Zaher, H.S. (2022). Canary in a coal mine: collided ribosomes as sensors of cellular conditions. Trends Biochem. Sci. *47*, 82–97. https://doi.org/10.1016/j.tibs.2021.09.001.

20. Pochopien, A.A., Beckert, B., Kasvandik, S., Berninghausen, O., Beckmann, R., Tenson, T., and Wilson, D.N. (2021). Structure of Gcn1 bound to stalled and colliding 80S ribosomes. Proc. Natl. Acad. Sci. USA *118*. e2022756118. https://doi.org/10.1073/pnas.2022756118.

21. Wu, C.C., Peterson, A., Zinshteyn, B., Regot, S., and Green, R. (2020). Ribosome collisions trigger General Stress responses to regulate cell fate. Cell *182*, 404–416.e14. https://doi.org/10.1016/j.cell.2020.06.006.

22. Yan, L.L., and Zaher, H.S. (2021). Ribosome quality control antagonizes the activation of the integrated stress response on colliding ribosomes. Mol. Cell *81*, 614–628.e4. https://doi.org/10.1016/j.molcel.2020.11.033.

23. Carelli, J.D., Sethofer, S.G., Smith, G.A., Miller, H.R., Simard, J.L., Merrick, W.C., Jain, R.K., Ross, N.T., and Taunton, J. (2015). Ternatin and improved synthetic variants kill cancer cells by targeting the elongation factor-1A ternary complex. eLife *4*, e10222. https://doi.org/10.7554/eLife.10222.

24. Shao, S., Murray, J., Brown, A., Taunton, J., Ramakrishnan, V., and Hegde, R.S. (2016). Decoding mammalian ribosome-mRNA states by translational GTPase complexes. Cell *167*, 1229–1240.e15. https://doi.org/10.1016/j.cell.2016.10.046.

25. Wang, H.-Y., Yang, H., Holm, M., Tom, H., Oltion, K., Al-Khdhairawi, A.A.Q., Weber, J.-F.F., Blanchard, S.C., Ruggero, D., and Taunton, J. (2022). Synthesis and single-molecule imaging reveal stereospecific enhancement of binding kinetics by the antitumor eEF1A antagonist SR-A3. Nat. Chem. *14*, 1443–1450. https://doi.org/10.1038/s41557-022-01039-3.

26. Juette, M.F., Carelli, J.D., Rundlet, E.J., Brown, A., Shao, S., Ferguson, A., Wasserman, M.R., Holm, M., Taunton, J., and Blanchard, S.C. (2022). Didemnin B and ternatin-4 inhibit conformational changes in eEF1A required for aminoacyl-tRNA accommodation into mammalian ribosomes. eLife *11*, e81608. https://doi.org/10.7554/eLife.81608.

27. Zecha, J., Meng, C., Zolg, D.P., Samaras, P., Wilhelm, M., and Kuster, B. (2018). Peptide level turnover measurements enable the study of proteoform dynamics. Mol. Cell. Proteomics *17*, 974–992. https://doi.org/10.1074/mcp.RA118.000583.

28. Budkevich, T., Giesebrecht, J., Altman, R.B., Munro, J.B., Mielke, T., Nierhaus, K.H., Blanchard, S.C., and Spahn, C.M.T. (2011). Structure and dynamics of the mammalian ribosomal pretranslocation complex. Mol. Cell *44*, 214–224. https://doi.org/10.1016/j.molcel.2011.07.040.

29. Fresno, M., Jiménez, A., and Vázquez, D. (1977). Inhibition of translation in eukaryotic systems by harringtonine. Eur. J. Biochem. *72*, 323–330. https://doi.org/10.1111/j.1432-1033.1977.tb11256.x.

30. Chen, J.J., Nathaniel, D.L., Raghavan, P., Nelson, M., Tian, R., Tse, E., Hong, J.Y., See, S.K., Mok, S.A., Hein, M.Y., et al. (2019). Compromised function of the ESCRT pathway promotes endolysosomal escape of tau seeds and propagation of tau aggregation. J. Biol. Chem. *294*, 18952–18966. https://doi.org/10.1074/jbc.RA119.009432.

31. Kampmann, M., Bassik, M.C., and Weissman, J.S. (2013). Integrated platform for genome-wide screening and construction of high-density genetic interaction maps in mammalian cells. Proc. Natl. Acad. Sci. USA *110*, E2317–E2326. https://doi.org/10.1073/pnas.1307002110.

32. Tian, R., Gachechiladze, M.A., Ludwig, C.H., Ward, M.E., Tian, R., Gachechiladze, M.A., Ludwig, C.H., Laurie, M.T., and Hong, J.Y. (2019). CRISPR interference-based platform for multimodal genetic screens in human iPSC-derived neurons. Neuron *104*, 239–255.e12. https://doi.org/10.1016/j.neuron.2019.07.014.

33. Kang, H.Y., Yeh, S., Fujimoto, N., and Chang, C. (1999). Cloning and characterization of human prostate coactivator ARA54, a novel protein that associates with the androgen receptor. J. Biol. Chem. *274*, 8570–8576. https://doi.org/10.1074/jbc.274.13.8570.

34. Walden, H., and Rittinger, K. (2018). RBR ligase-mediated ubiquitin transfer: A tale with many twists and turns. Nat. Struct. Mol. Biol. *25*, 440–445. https://doi.org/10.1038/s41594-018-0063-3.

35. Dove, K.K., and Klevit, R.E. (2017). RING-between-RING E3 ligases: emerging themes amid the variations. J. Mol. Biol. *429*, 3363–3375. https://doi.org/10.1016/j.jmb.2017.08.008.

36. Lorick, K.L., Jensen, J.P., Fang, S., Ong, A.M., Hatakeyama, S., and Weissman, A.M. (1999). Ring fingers mediate ubiquitin-conjugating enzyme (E2)-dependent ubiquitination. Proc. Natl. Acad. Sci. USA *96*, 11364–11369. https://doi.org/10.1073/pnas.96.20.11364.

37. Hundley, F.V., Sanvisens Delgado, N., Marin, H.C., Carr, K.L., Tian, R., and Toczyski, D.P. (2021). A comprehensive phenotypic CRISPR-Cas9 screen of the ubiquitin pathway uncovers roles of ubiquitin ligases in mitosis. Mol. Cell *81*, 1319–1336.e9. https://doi.org/10.1016/j.molcel.2021.01.014.

38. Kim, W., Bennett, E.J., Huttlin, E.L., Guo, A., Li, J., Possemato, A., Sowa, M.E., Rad, R., Rush, J., Comb, M.J., et al. (2011). Systematic and quantitative assessment of the ubiquitin-modified proteome. Mol. Cell *44*, 325–340. https://doi.org/10.1016/j.molcel.2011.08.025.

39. Elia, A.E.H., Boardman, A.P., Wang, D.C., Huttlin, E.L., Everley, R.A., Dephoure, N., Zhou, C., Koren, I., Gygi, S.P., and Elledge, S.J. (2015). Quantitative proteomic atlas of ubiquitination and acetylation in the DNA damage response. Mol. Cell *59*, 867–881. https://doi.org/10.1016/j.molcel.2015.05.006.

40. Heidelberger, J.B., Voigt, A., Borisova, M.E., Petrosino, G., Ruf, S., Wagner, S.A., and Beli, P. (2018). Proteomic profiling of VCP substrates links VCP to K6-linked ubiquitylation and c-Myc function. EMBO Rep. *19*, 1–20. https://doi.org/10.15252/embr.201744754.

41. Sundaramoorthy, E., Leonard, M., Mak, R., Liao, J., Fulzele, A., and Bennett, E.J. (2017). ZNF598 and RACK1 regulate mammalian ribosome-associated quality control function by mediating regulatory 40S ribosomal ubiquitylation. Mol. Cell *65*, 751–760.e4. https://doi.org/10.1016/j.molcel.2016.12.026.

42. Garzia, A., Jafarnejad, S.M., Meyer, C., Chapat, C., Gogakos, T., Morozov, P., Amiri, M., Shapiro, M., Molina, H., Tuschl, T., et al. (2017). The E3 ubiquitin ligase and RNA-binding protein ZNF598 orchestrates ribosome quality control of premature polyadenylated mRNAs. Nat. Commun. *8*, 16056. https://doi.org/10.1038/ncomms16056.

43. Deshar, R., Moon, S., Yoo, W., Cho, E.B., Yoon, S.K., and Yoon, J.B. (2016). RNF167 targets Arl8B for degradation to regulate lysosome positioning and endocytic trafficking. FEBS Journal *283*, 4583–4599. https://doi.org/10.1111/febs.13947.

44. Yoo, W., Cho, E.B., Kim, S., and Yoon, J.B. (2019). The E3 ubiquitin ligase March2 regulates ERGIC3-dependent trafficking of secretory proteins. J. Biol. Chem. *294*, 10900–10912. https://doi.org/10.1074/jbc.RA119.007435.

45. Deshar, R., Yoo, W., Cho, E.B., Kim, S., and Yoon, J.B. (2019). RNF8 mediates NONO degradation following UV-induced DNA damage to properly terminate ATR-CHK1 checkpoint signaling. Nucleic Acids Res. *47*, 762–778. https://doi.org/10.1093/nar/gky1166.

46. Sattlegger, E., and Hinnebusch, A.G. (2000). Separate domains in GCN1 for binding protein kinase GCN2 and ribosomes are required for GCN2 activation in amino acid-starved cells. EMBO J. *19*, 6622–6633. https://doi.org/10.1093/emboj/19.23.6622.

47. Kubota, H., Sakaki, Y., and Ito, T. (2000). GI domain-mediated association of the eukaryotic initiation factor 2alpha kinase GCN2 with its activator GCN1 is required for general amino acid control in budding yeast. J. Biol. Chem. *275*, 20243–20246. https://doi.org/10.1074/jbc.C000262200.

48. Sattlegger, E., and Hinnebusch, A.G. (2005). Polyribosome binding by GCN1 is required for full activation of eukaryotic translation initiation factor 2α kinase GCN2 during amino acid starvation. J. Biol. Chem. *280*, 16514–16521. https://doi.org/10.1074/jbc.M414566200.

49. Meydan, S., and Guydosh, N.R. (2020). Disome and trisome profiling reveal genome-wide targets of ribosome quality control. Mol. Cell *79*, 588–602.e6. https://doi.org/10.1016/j.molcel.2020.06.010.

50. Castilho, B.A., Shanmugam, R., Silva, R.C., Ramesh, R., Himme, B.M., and Sattlegger, E. (2014). Keeping the eIF2 alpha kinase Gcn2 in check. Biochim. Biophys. Acta *1843*, 1948–1968. https://doi.org/10.1016/j.bbamcr.2014.04.006.

51. Sharma, J., Du, M., Wong, E., Mutyam, V., Li, Y., Chen, J., Wangen, J., Thrasher, K., Fu, L., Peng, N., et al. (2021). A small molecule that induces translational readthrough of CFTR nonsense mutations by eRF1 depletion. Nat. Commun. *12*, 4358. https://doi.org/10.1038/s41467-021-24575-x.

52. Michel, M.A., Swatek, K.N., Hospenthal, M.K., and Komander, D. (2017). Ubiquitin linkage-specific affimers reveal insights into K6-linked ubiquitin signaling. Mol. Cell *68*, 233–246.e5. https://doi.org/10.1016/j.molcel.2017.08.020.

53. Brown, A., Shao, S., Murray, J., Hegde, R.S., and Ramakrishnan, V. (2015). Structural basis for stop codon recognition in eukaryotes. Nature *524*, 493–496. https://doi.org/10.1038/nature14896.

54. Garzia, A., Meyer, C., and Tuschl, T. (2021). The E3 ubiquitin ligase RNF10 modifies 40S ribosomal subunits of ribosomes compromised in translation. Cell Rep. *36*, 109468. https://doi.org/10.1016/j.celrep.2021.109468.

55. Garshott, D.M., An, H., Sundaramoorthy, E., Leonard, M., Vicary, A., Harper, J.W., and Bennett, E.J. (2021). iRQC, a surveillance pathway for 40S ribosomal quality control during mRNA translation initiation. Cell Rep. *36*, 109642. https://doi.org/10.1016/j.celrep.2021.109642.

56. Montellese, C., van den Heuvel, J., Ashiono, C., Dörner, K., Melnik, A., Jonas, S., Zemp, I., Picotti, P., Gillet, L.C., and Kutay, U. (2020). USP16 counteracts mono-ubiquitination of RPS27a and promotes maturation of the 40S ribosomal subunit. eLife *9*, e54435. https://doi.org/10.7554/eLife.54435.

57. Sinha, N.K., Ordureau, A., Best, K.M., Saba, J.A., Zinshteyn, B., Sundaramoorthy, E., Fulzele, A., Garshott, D.M., Denk, T., Thoms, M., et al. (2020). EDF1 coordinates cellular responses to ribosome collisions. eLife *9*, e58828. https://doi.org/10.7554/eLife.58828.

58. Cotton, T.R., and Lechtenberg, B.C. (2020). Chain reactions: molecular mechanisms of RBR ubiquitin ligases. Biochem. Soc. Trans. *48*, 1737–1750. https://doi.org/10.1042/BST20200237.

59. Wainberg, M., Kamber, R.A., Balsubramani, A., Meyers, R.M., Sinnott-Armstrong, N., Hornburg, D., Jiang, L., Chan, J., Jian, R., Gu, M., et al. (2021). A genome-wide atlas of co-essential modules assigns function to uncharacterized genes. Nat. Genet. *53*, 638–649. https://doi.org/10.1038/s41588-021-00840-z.

60. Hawer, H., Hammermeister, A., Ravichandran, K.E., Glatt, S., Schaffrath, R., and Klassen, R. (2018). Roles of elongator dependent tRNA modification pathways in neurodegeneration and cancer. Genes (Basel) *10*, 1–23. https://doi.org/10.3390/genes10010019.

61. Hermand, D. (2020). Anticodon wobble uridine modification by elongator at the crossroad of cell signaling, differentiation, and diseases. Epigenomes *4*, 7. https://doi.org/doi:. https://doi.org/10.3390/epigenomes4020007

62. Urakov, V.N., Valouev, I.A., Lewitin, E.I., Paushkin, S.V., Kosorukov, V.S., Kushnirov, V.V., Smirnov, V.N., and Ter-Avanesyan, M.D. (2001). Itt1p, a novel protein inhibiting translation termination in Saccharomyces cerevisiae. BMC Mol. Biol. *2*, 9. https://doi.org/10.1186/1471-2199-2-9.

63. Yamazaki, H., Kasai, S., Mimura, J., Ye, P., Inose-Maruyama, A., Tanji, K., Wakabayashi, K., Mizuno, S., Sugiyama, F., Takahashi, S., et al. (2020). Ribosome binding protein GCN1 regulates the cell cycle and cell proliferation and is essential for the embryonic development of mice. PLoS Genet. *16*, e1008693. https://doi.org/10.1371/journal.pgen.1008693.

64. Zhang, P., McGrath, B.C., Reinert, J., Olsen, D.S., Lei, L.L., Gill, S., Wek, S.A., Vattem, K.M., Wek, R.C., Kimball, S.R., et al. (2002). The GCN2 eIF2 kinase is required for adaptation to amino acid deprivation in mice. Mol. Cell. Biol. *22*, 6681–6688. https://doi.org/10.1128/MCB.22.19.6681-6688.2002.

65. Sattlegger, E., Swanson, M.J., Ashcraft, E.A., Jennings, J.L., Fekete, R.A., Link, A.J., and Hinnebusch, A.G. (2004). YIH1 is an actin-binding protein that inhibits protein kinase GCN2 and impairs general amino acid control when overexpressed. J. Biol. Chem. *279*, 29952–29962. https://doi.org/10.1074/jbc.M404009200.

66. Wout, P.K., Sattlegger, E., Sullivan, S.M., and Maddock, J.R. (2009). Saccharomyces cerevisiae Rbg1 protein and its binding partner gir2 interact on polyribosomes with Gcn1. Eukaryot. Cell *8*, 1061–1071. https://doi.org/10.1128/EC.00356-08.

67. Liu, J., Xu, Y., Stoleru, D., and Salic, A. (2012). Imaging protein synthesis in cells and tissues with an alkyne analog of puromycin. Proc. Natl. Acad. Sci. USA *109*, 413–418. https://doi.org/10.1073/pnas.1111561108.

68. Krastel, P., Roggo, S., Schirle, M., Ross, N.T., Perruccio, F., Aspesi, P., Jr., Aust, T., Buntin, K., Estoppey, D., Liechty, B., et al. (2015). Nannocystin A: an elongation Factor 1 inhibitor from myxobacteria with differential anti-cancer properties. Angew. Chem. *127*, 10287–10292. https://doi.org/10.1002/anie.201505069.

69. Horlbeck, M.A., Gilbert, L.A., Villalta, J.E., Adamson, B., Pak, R.A., Chen, Y., Fields, A.P., Park, C.Y., Corn, J.E., Kampmann, M., et al. (2016). Compact and highly active next-generation libraries for CRISPR-mediated gene repression and activation. eLife *5*, 1–20. https://doi.org/10.7554/eLife.19760.

Cell
Article

CellPress

70. Ran, F.A., Hsu, P.D., Wright, J., Agarwala, V., Scott, D.A., and Zhang, F. (2013). Genome engineering using the CRISPR-Cas9 system. Nat. Protoc. *8*, 2281–2308. https://doi.org/10.1038/nprot.2013.143.

71. Cox, J., and Mann, M. (2008). MaxQuant enables high peptide identification rates, individualized p.p.b.-range mass accuracies and proteome-wide protein quantification. Nat. Biotechnol. *26*, 1367–1372. https://doi.org/10.1038/nbt.1511.

72. MacLean, B., Tomazela, D.M., Shulman, N., Chambers, M., Finney, G.L., Frewen, B., Kern, R., Tabb, D.L., Liebler, D.C., and MacCoss, M.J. (2010). Skyline: an open source document editor for creating and analyzing targeted proteomics experiments. Bioinformatics *26*, 966–968. https://doi.org/10.1093/bioinformatics/btq054.

73. Spandidos, A., Wang, X., Wang, H., and Seed, B. (2010). PrimerBank: a resource of human and mouse PCR primer pairs for gene expression detection and quantification. Nucleic Acids Res. *38*, D792–D799. https://doi.org/10.1093/nar/gkp1005.

74. Udeshi, N.D., Svinkina, T., Mertins, P., Kuhn, E., Mani, D.R., Qiao, J.W., and Carr, S.A. (2013). Refined Preparation and Use of Anti-diglycine Remnant (K-ε-GG) antibody Enables Routine Quantification of 10,000s of ubiquitination Sites in Single proteomics Experiments. Mol. Cell. Proteomics *12*, 825–831. https://doi.org/10.1074/mcp.O112.027094.

75. Shi, Z., Fujii, K., Kovary, K.M., Genuth, N.R., Röst, H.L., Teruel, M.N., and Barna, M. (2017). Heterogeneous ribosomes preferentially translate distinct subpools of mRNAs genome-wide. Mol. Cell *67*, 71–83.e7. https://doi.org/10.1016/j.molcel.2017.05.021.

STAR★METHODS

KEY RESOURCES TABLE

Reagent or Resource	Source	Identifiers
Antibodies		
Mouse monoclonal anti-eEF1A, clone CBP-KK1	EMD Millipore	Cat# 05-235; RRID: AB_309663
Rabbit monoclonal anti-beta Actin (13E5)	Cell Signaling Technology	Cat# 4970S; RRID: AB_2223172
Mouse monoclonal anti-RNF14 (B-10)	Santa Cruz Biotechnology	Cat# sc-376701; RRID: AB_11150281
Rabbit polyclonal anti-RNF25	Abcam	Cat# ab140514
Rabbit monoclonal anti-V5 (D3H8Q)	Cell Signaling Technologies	Cat# 13202S; RRID: AB_2687461
Mouse monoclonal anti-Flag	Sigma-Aldrich	Cat# F3165; RRID: AB_259529
Mouse monoclonal anti-HA (6E2)	Cell Signaling Technologies	Cat# 2367S; RRID: AB_10691311
Rabbit polyclonal anti-GCN1L1	Novus Biologicals	Cat# NBP1-83383; RRID: AB_11022056
Rabbit polyclonal anti-GCN2	Cell Signaling Technologies	Cat# 3302S; RRID: AB_2277617
Rabbit polyclonal anti-RPL7	Bethyl Laboratories	Cat# A300-741A; RRID: AB_2301241
Rabbit polyclonal anti-RPS13	Proteintech	Cat# 16680-1-AP; RRID: AB_2182500
Mouse monoclonal anti-eRF1 (B-11)	Santa Cruz Biotechnology	Cat# sc-365686; RRID: AB_10843214
Chicken polyclonal anti-GFP	Abcam	Cat# ab13970; RRID: AB_300798
Rat monoclonal APC anti-Flag	BioLegend	Cat# 637307; RRID: AB_2561496
Goat polyclonal anti-mouse IgG IRDye 680RD	LI-COR	Cat# 926-68070; RRID: AB_10956588
Goat polyclonal anti-mouse IgG IRDye 800CW	LI-COR	Cat# 926-32210; RRID: AB_621842
Goat polyclonal anti-rabbit IgG IRDye 680RD	LI-COR	Cat# 926-68071; RRID: AB_10956166
Goat polyclonal anti-rabbit IgG IRDye 800CW	LI-COR	Cat# 926-32211; RRID: AB_621843
Donkey polyclonal anti-chicken IgG IRDye 800CW	LI-COR	Cat# 925-32218; RRID: AB_2814922
Chemicals, Peptides, and Recombinant Proteins		
Ternatin-4	Wang et al.[25]	n/a
Cycloheximide	Sigma-Aldrich	Cat# C7698
Homoharringtonine	MedChemExpress	Cat# HY-14944
Carfilzomib	Abcam	Cat# ab216469
CB-5083	ApexBio	Cat# B6032
SRI-41315	ProbeChem	n/a
O-propargyl puromycin (OPP)	Liu et al.[67]	n/a
Puromycin	InvivoGen	Cat# ant-pr-1
Biotin	Sigma-Aldrich	Cat# B4501
Chloroacetamide	Sigma-Alrich	Cat# 22790
$^{13}C_6$ $^{15}N_4$ L-arginine hydrochloride	Cambridge Isotope Laboratories	Cat# CNLM-539-H-0.1
$^{13}C_6$ $^{15}N_2$ L-lysine hydrochloride	Cambridge Isotope Laboratories	Cat# CNLM-291-H-0.1
Zombie Aqua Fixable Viability Kit	BioLegend	Cat# 423101
CF647 azide	Biotium	Cat# 92084
eEF1A K385 standard peptide SGK[diGly]KLEDGPK, with 13C6,15N-Leu	Peptide Specialty Laboratories	n/a
3xFlag Peptide	Sigma-Aldrich	Cat# M4799
EDTA-free Protease Inhibitor Cocktail	Roche	Cat# 11873580001
Q5 Hot Start PCR Master Mix	New England Biolabs	Cat# M094
RNase Inhibitor, Human Placenta	New England Biolabs	Cat# M0307
SUPERaseIn RNase Inhibitor	Invitrogen	Cat# AM2694
Micrococcal nuclease	Roche	Cat# 10107921001
TURBO DNase	Invitrogen	Cat# AM2238

(*Continued on next page*)

Cell
Article

CellPress

Continued		
Reagent or Resource	Source	Identifiers
Trypsin	Promega	Cat# V5113
IRDye 800CW Streptavidin	LI-COR	Cat# 926-32230
Pierce Streptavidin Magnetic Beads	Thermo Fisher Scientific	Cat# 88817
Anti-Flag M2 Magnetic Beads	Sigma-Aldrich	Cat# M8823
Anti-Ubiquitin Lys6 specific GFP/His-tag Affimer	EMD Millipore	Cat# MABS1918
GFP-Trap Magnetic Agarose	ChromoTek	Cat# gtma
Mirus TransIT-LT1 Transfection Reagent	Mirus Bio	Cat# MIR2300
Lipofectamine 2000	Invitrogen	Cat# 11668-019
Lipofectamine LTX	Invitrogen	Cat# 15338030
ViralBoost Reagent	Alstem Cell Advancements	Cat# VB100
Hexadimethrine bromide (polybrene)	Sigma-Aldrich	Cat# TR-1003-G
16% Paraformaldehyde Solution	Electron Microscopy Sciences	Cat# 15710
Critical Commercial Assays		
NucleoSpin Blood L Kit	Macherey-Nagel	Cat# 740954.20
PTMScan® Ubiquitin Remnant Motif (K-ε-GG) Kit	Cell Signaling Technology	Cat# 5562
RNeasy Mini Kit	Qiagen	Cat# 74104
High-Capacity cDNA Reverse Transcription Kit	Applied Biosystems	Cat# 4368813
Luna Universal qPCR Master Mix	New England Biolabs	Cat# M3003
Deposited data		
Digly proteomics data	This paper	MassIVE: MSV000090779; ProteomeXchange: PXD038340
Experimental Models: Cell Lines		
HeLa	ATCC	CCL-2
HEK293T	ATCC	CRL-3216
HCT116 eEF1A1 A399V/A399V	Krastel et al.[68]	N/A
HCT116 eEF1A1 A399V/A399V Flag-mCherry-eEF1A1_IRES-GFP dCas9-HA-NLS-BFP-KRAB	This paper	N/A
HCT116 eEF1A1 A399V/A399V Flag-mCherry-eEF1A1_IRES-GFP	This paper	N/A
HCT116 eEF1A1 A399V/A399V Flag-mCherry-eEF1A1 A399V_IRES-GFP	This paper	N/A
HCT116 eEF1A1 A399V/A399V Flag-mCherry-eEF1A1 K212R_IRES-GFP	This paper	N/A
HCT116 eEF1A1 A399V/A399V Flag-mCherry-eEF1A1 K273R_IRES-GFP	This paper	N/A
HCT116 eEF1A1 A399V/A399V Flag-mCherry-eEF1A1 K385R_IRES-GFP	This paper	N/A
HCT116 eEF1A1 A399V/A399V Flag-mCherry-eEF1A1 K395R_IRES-GFP	This paper	N/A
HCT116 eEF1A1 A399V/A399V Flag-mCherry-eEF1A1 K408R_IRES-GFP	This paper	N/A
HCT116 eEF1A1 A399V/A399V 3xFlag-eEF1A1	This paper	N/A
HCT116 eEF1A1 A399V/A399V 3xFlag-eEF1A1 K385R	This paper	N/A
HeLa RNF14 KO	This paper	N/A
HeLa RNF25 KO	This paper	N/A
HeLa RNF14 KO V5-RNF14	This paper	N/A
HeLa RNF14 KO V5-RNF14 C417A	This paper	N/A
HeLa RNF25 KO V5-RNF25	This paper	N/A
HeLa RNF25 KO V5-RNF25 dRING (aa 135-201)	This paper	N/A
HeLa V5-RNF14	This paper	N/A

Continued

Reagent or Resource	Source	Identifiers
HeLa V5-RNF14 C417A	This paper	N/A
HeLa V5-RNF25	This paper	N/A
HeLa V5-RNF25 dRING (aa 135-201)	This paper	N/A
HeLa 3xFlag-TEV-RNF14	This paper	N/A
HeLa 3xFlag-TEV-RNF14 C417A	This paper	N/A
HeLa 3xFlag-TEV-RNF25	This paper	N/A
HeLa dCas9-HA-NLS-BFP-KRAB	This paper	N/A
HeLa RPS27A-3xFlag dCas9-HA-NLS-BFP-KRAB	This paper	N/A
HeLa RPS27A K113R-3xFlag dCas9-HA-NLS-BFP-KRAB	This paper	N/A
HeLa RPS27A K107/113R-3xFlag dCas9-HA-NLS-BFP-KRAB	This paper	N/A
HeLa V5-RNF14 RPS27A-3xFlag dCas9-HA-NLS-BFP-KRAB	This paper	N/A
HeLa V5-RNF14 RPS27A K113R-3xFlag dCas9-HA-NLS-BFP-KRAB	This paper	N/A
HeLa V5-RNF25 RPS27A-3xFlag dCas9-HA-NLS-BFP-KRAB	This paper	N/A
HeLa V5-RNF25 RPS27A K113R-3xFlag dCas9-HA-NLS-BFP-KRAB	This paper	N/A
Oligonucleotides		
See Table S3	This paper	n/a
Recombinant DNA		
pLX304 Flag-mCherry-eEF1A1_IRES-GFP	This paper	N/A
pLX302 Flag-mCherry-eEF1A1_IRES-GFP	This paper	N/A
pLX302 Flag-mCherry-eEF1A1 A399V_IRES-GFP	This paper	N/A
pLX302 Flag-mCherry-eEF1A1 K212R_IRES-GFP	This paper	N/A
pLX302 Flag-mCherry-eEF1A1 K273R_IRES-GFP	This paper	N/A
pLX302 Flag-mCherry-eEF1A1 K385R_IRES-GFP	This paper	N/A
pLX302 Flag-mCherry-eEF1A1 K395R_IRES-GFP	This paper	N/A
pLX302 Flag-mCherry-eEF1A1 K408R_IRES-GFP	This paper	N/A
pLX302 3xFlag-eEF1A1_IRES-GFP	This paper	N/A
pLX302 3xFlag-eEF1A1 K385R_IRES-GFP	This paper	N/A
pHR V5-RNF14_IRES-mCherry	This paper; RNF14 sequence from DNASU Clone # HsCD00436670	N/A
pHR V5-RNF14 C417A_IRES-mCherry	This paper	N/A
pHR V5-RNF25_IRES-mCherry	This paper; RNF25 sequence from DNASU Clone # HsCD00438677	N/A
pHR V5-RNF25 dRING (aa 135-201)_IRES-mCherry	This paper	N/A
pHR V5-BirA_IRES-mCherry	This paper; BirA sequence from Deshar et al.[43]	N/A
pHR V5-BirA-RNF14_IRES-mCherry	This paper	N/A
pHR V5-BirA-RNF14 C417A_IRES-mCherry	This paper	N/A
pHR V5-BirA-RNF25_IRES-mCherry	This paper	N/A
pHR V5-BirA-RNF25 dRING (aa 135-201)_IRES-mCherry	This paper	N/A
pHR 3xFlag-TEV-RNF14_IRES-mCherry	This paper	N/A
pHR 3xFlag-TEV-RNF14 C417A_IRES-mCherry	This paper	N/A
pHR 3xFlag-TEV-RNF25_IRES-mCherry	This paper	N/A
pLenti6.3 GCN1-3xFlag_IRES-iRFP	This paper; GCN1 sequence from DNASU Clone # HsCD00946315	N/A
pLenti6.3 GCN1 R2312A-3xFlag_IRES-iRFP	This paper	N/A
pHR RPS27A-3xFlag_IRES-AcGFP	This paper; RPS27A sequence from Addgene Plasmid #69561	N/A

Cell
Article

🔗 **CellPress**

Continued

Reagent or Resource	Source	Identifiers
pHR RPS27A K113R-3xFlag_IRES-AcGFP	This paper	N/A
pHR RPS27A K107/113R-3xFlag_IRES-AcGFP	This paper	N/A
pHR RPS27A-3xFlag_IRES-iRFP	This paper	N/A
pHR RPS27A K107R-3xFlag_IRES-iRFP	This paper	N/A
pHR RPS27A K113R-3xFlag_IRES-iRFP	This paper	N/A
pHR RPS27A K107/113R-3xFlag_IRES-iRFP	This paper	N/A
pLX304 3xFlag-eRF1_IRES-AcGFP	This paper	N/A
pLX304 3xFlag-eRF1 G183/184A_IRES-AcGFP	This paper	N/A
pcDNA3.1 AP-HA-Ub	Deshar et al.[43]	N/A
pHR dCas9-HA-NLS-BFP-KRAB	Innovative Genomics Institute	Plasmid #IGI_P0152
pLG15	Horlbeck et al.[69]	N/A
CRISPRi UPS pooled library	Chen et al.[30]	N/A
pCMV-dR8.91	Gift from Didier Trono	Addgene Ref #2221
pMD2.G	Gift from Didier Trono	Addgene Plasmid #12259
PX458 pSpCas9(BB)-2A-GFP	Ran et al.[70]	Addgene Plasmid #48138
Software and Algorithms		
GraphPad Prism	GraphPad Prism software	N/A
Image Studio Lite	LI-COR	N/A
FlowJo	BD Biosciences	N/A
Tableau	Tableau software	N/A
MaxQuant	Cox and Mann[71]	N/A
Skyline	MacLean et al.[72]	N/A
Adobe Illustrator	Adobe	N/A
Adobe Photoshop	Adobe	N/A

RESOURCE AVAILABILITY

Lead contact
Further information and requests for reagents should be directed to the lead contact, Jack Taunton (jack.taunton@ucsf.edu).

Materials availability
Plasmids and cell lines generated in this study are available upon request from the lead contact.

Data and code availability
- All mass spectrometry raw files have been deposited into the MassIVE database and in ProteomeXchange. Accession numbers are listed in the key resources table.
- This paper does not report original code.
- Any additional information required to reanalyze the data reported in this paper is available from the lead contact upon request.

EXPERIMENTAL MODEL AND SUBJECT DETAILS

Cell lines and culture conditions
HEK293T and HeLa cells were maintained in Dulbecco's Modified Eagle's Medium (DMEM) supplemented with 10% fetal bovine serum (FBS), 100 U/mL penicillin, and 100 μg/mL streptomycin. HCT116 eEF1A1 A399V/A399V cells were previously described[68] and were maintained in McCoy's media supplemented with 10% FBS, 100 U/mL penicillin, and 100 μg/mL streptomycin. Antibiotics were omitted for all transfection-based experiments. Cells were grown in a humidified incubator at 37 °C with a 5% CO_2 atmosphere. Unless indicated otherwise, all treatment conditions utilized a vehicle control, 50 nM ternatin-4, 10 μM SRI-41315, 50 μg/mL cyclo-heximide, 2 μg/mL homoharringtonine, 500 nM carfilzomib or 2.5 μM CB-5083 as described in figure legends. Ultraviolet irradiation was conducted using a Stratagene UV Stratalinker 2400 as follows: cells were washed once with DPBS (containing Ca^{+2}/Mg^{+2}), dry plates were irradiated with 40 J/m^2 UV-C, fresh media was added to plates, and cells were returned to the incubator for a 1 h recovery period. Treatment proceeded identically for control samples, except dishes were covered with cardboard during irradiation.

METHOD DETAILS

Plasmid Generation

Plasmids encoding the indicated genes, epitope tags, and IRES sequences were constructed by Gibson cloning. Point mutations and the RNF25 RING deletion (residues 135-201) were created by site-directed mutagenesis. All eEF1A1-encoding constructs were expressed from a pLX302 vector containing IRES-AcGFP, except the mCherry-eEF1A1 reporter used for the CRISPRi screen, which was expressed from a pLX304 vector. RNF14, RNF25, and RPS27A-encoding constructs were expressed from a pHR vector containing IRES-mCherry (RNF14 and RNF25) or IRES-AcGFP or iRFP (RPS27A). GCN1 was expressed in a modified pLenti6.3 vector with the SV40 promoter and blasticidin resistance marker removed, and IRES-iRFP added. eRF1 was expressed from a pLX304 vector containing IRES-AcGFP. Plasmids encoding individual sgRNAs were constructed by ligating complementary oligonucleotides (sequences indicated above in **Sequence-Based Reagents**) into the BlpI and BstXI restriction enzyme sites of pLG15 (CRISPRi) or the BbsI restriction enzyme sites of PX458 (CRISPR KO). All plasmids were verified by Sanger sequencing.

Lentivirus and stable cell line generation

Lentivirus was generated by transfecting HEK293T cells growing at approximately 60% confluency in 6-well dishes with lipid complexes containing 1.5 μg of a construct of interest, 1.35 μg pCMV-dR8.91, 165 ng pMD2-G, and 7.5 μL Mirus TransIT-LT1 diluted in Opti-MEM. Alstem ViralBoost was added to cells after addition of the transfection mix. Two days post-transfection, an additional 1.5 mL complete DMEM was added to cells. The viral supernatant was collected on the third day and filtered through 0.45 μm sterile SFCA syringe filters (Thermo Scientific). Supernatant was used immediately or stored at -20 °C.

For stable cell line generation, media containing 8 μg/mL polybrene was added to cells, lentivirus was added, and cells were incubated overnight. Lentivirus was removed from cells, and cells were expanded until cell sorting using a BD FACS Aria II. Transduced cells were typically sorted to at least 95% purity.

CRISPR knockout cell lines

CRISPR knockout cells were generated as previously described.[70] sgRNA sequences targeting exon 5 of RNF14 and exon 3 of RNF25 were identified using the Broad CRISPR design tool (crispr.mit.edu/v1) and ligated into the PX458 (pSpCas9(BB)-2A-GFP) plasmid. HeLa cells were transfected using Lipofectamine 2000 and sorted for GFP positivity after 3 days. Eight days post-transfection, cells were plated into a 96-well plate at 0.5 cells per well. After appearance of visible colonies (approximately 2 weeks), wells containing individual colonies were collected by trypsinization and expanded to 6-well dishes. Clones were screened for RNF14/RNF25 expression by Western blotting and Sanger sequencing prior to selection for experiments.

Immunoblot analysis

Cells were washed once with ice-cold PBS and stored at -80 °C or immediately lysed using lysis buffer (50 mM HEPES pH 7.4, 150 mM NaCl, 1% NP-40, 2x Roche EDTA-free protease inhibitors). Lysates were collected by scraping and were cleared by centrifugation at 16,100 g for 10 minutes at 4 °C. Total protein was quantified using the Bradford method and normalized prior to electrophoresis using hand-cast 7.5% polyacrylamide gels. Proteins were transferred to 0.45 μm nitrocellulose membranes (Bio-Rad) using a Bio-Rad Criterion transfer system. Membranes were blocked for 1 hour at room temperature using blocking buffer (5% BSA, 0.1% sodium azide in TBS-T). Membranes were incubated with primary antibodies diluted in blocking buffer for 1 hour at room temperature or overnight at 4 °C. Membranes were rinsed with TBS-T (3 x 5 minutes at room temperature) and incubated with secondary antibodies diluted in blocking buffer for 1 hour at room temperature. Membranes were rinsed with TBS-T (3 x 5 minutes at room temperature) and were imaged using a Li-Cor Odyssey system.

Protein synthesis measurements

Cells were grown to 70% confluency in 12-well plates and treated as indicated (ternatin-4 or vehicle; 20 h). Following treatment, O-propargyl puromycin (OPP) was added to all wells at a final concentration of 30 μM, and cells were incubated for an additional hour. Cells were collected by trypsinization and transferred to a 96-well V-bottom plate for the remainder of the experiment. All centrifugation steps were performed at 2,100 g for 3 minutes at 4 °C, and all washes and incubations were done with 200 μL buffer unless indicated otherwise. Cells were washed once with cold PBS and then stained with 100 μL Zombie Aqua (BioLegend; 1:1000 in PBS) for 30 min at RT. Incubations from this step onwards were performed in the dark. Cells were washed once (2% FBS in PBS) and fixed with 4% paraformaldehyde (PFA) in PBS for 15 min at 4 °C. Cells were washed once (2% FBS in PBS) and incubated in permeabilization buffer (3% FBS, 0.1% saponin in PBS) for 5 min at RT. Click chemistry mix was prepared by adding the following components to final concentrations in the order listed: 50 mM HEPES pH 7.5, 150 mM NaCl, 400 μM TCEP, 250 μM TBTA, 5 μM CF647 azide (Biotium), 200 μM CuSO$_4$. Cells were resuspended in 25 μL permeabilization buffer, 100 μL click chemistry mix was added, and cells were incubated overnight at RT. Cells were washed twice with permeabilization buffer and twice with FACS buffer (2% FBS, 100 U/mL penicillin, 100 μg/mL streptomycin, and 2 mM EDTA in PBS lacking Ca^{+2}/Mg^{+2}). Samples were analyzed on a Thermo Attune NxT (see below). Data was processed in FlowJo (BD) with a gating hierarchy as follows: debris were excluded (FSC-H vs. SSC-A), doublets were excluded (FSC-H vs. FSC-W), and dead cells were excluded on the basis of Zombie Aqua positivity. Mean fluorescent intensity (MFI) was calculated for each sample and normalized to vehicle control samples.

Cell
Article

CellPress

Flag-APC cell staining

Cells growing in 6-well dishes were scraped into PBS. All centrifugation steps were performed at 2,100 g for 3 minutes at 4°C, and all washes and incubations were done with 200 μL buffer unless indicated otherwise. Cells were washed once (2% FBS in PBS) and fixed with 4% paraformaldehyde (PFA) in PBS for 15 min at RT. Cells were washed once (2% FBS in PBS) and incubated in permeabilization buffer (3% FBS, 0.1% saponin in PBS) for 5 min at RT. Cells were resuspended in 100 μL permeabilization buffer containing 0.1 μg APC-conjugated Flag antibody (BioLegend) and incubated in the dark for 30 min at RT. Cells were washed twice with permeabilization buffer and resuspended in FACS buffer (2% FBS, 100 U/mL penicillin, 100 μg/mL streptomycin, and 2 mM EDTA in PBS lacking Ca^{+2}/Mg^{+2}).

Flow cytometry

Cells were harvested by trypsinization, transferred to 96-well V-bottom plates, centrifuged at 2,100 g for 3 minutes at 4 °C, and re-suspended in FACS buffer (2% FBS, 100 U/mL penicillin, 100 μg/mL streptomycin, and 2 mM EDTA in PBS lacking Ca^{+2}/Mg^{+2}). Samples were analyzed using a Thermo Attune NxT equipped with 405 nm, 488 nm, 561 nm, and 637 nm lasers, except in Figure 7D, which utilized a BD CytoFlex S equipped with 405 nm, 488 nm, 561 nm, and 638 nm lasers. Single cells were analyzed using FlowJo (BD) software. For all samples, debris (FSC-H vs. SSC-A), and doublets (FSC-H vs. FSC-W) were excluded.

CRISPRi screen

CRISPRi screening cells were generated by transducing ternatin-resistant HCT116 eEF1A1 A399V/A399V cells with lentivirus encoding dCas9-HA-NLS-BFP-KRAB. Cells were sorted twice for BFP positivity. The resulting dCas9-containing cells were transduced with the eEF1A FACS reporter (pLX304 Flag-mCherry-eEF1A1_IRES-AcGFP) and were sorted twice for GFP positivity.

Throughout the screen, a minimum of 1000x representation was maintained for sgRNA elements. A sgRNA library targeting elements of the ubiquitin proteasome system[30] (9,564 sgRNAs total) was utilized. Several sgRNAs targeting additional eEF1A or RQC-related genes (*EF1A1*, *EF1A2*, *HBS1L*, *PELO*, *NEMF*, *TCF25*, *PUM2*, *PCBP1*) were individually cloned (5 sgRNAs/gene) and added to the library. Lentivirus was generated by transfecting two 15 cm dishes of HEK293T cells each with 9 μg of library, 8 μg of pCMV-dR8.91, and 1 μg of pMD2-G per dish using Mirus Trans-IT LT1 and Alstem ViralBoost. Viral supernatant was collected after two days and filtered. Six 15 cm dishes of CRISPRi screening cells were transduced with all freshly harvested virus, yielding a trans-duction efficiency of approximately 55% (measured by FACS two days post-transduction). Puromycin selection for sgRNA-containing cells began three days post-transduction and was conducted for 48 hours, with daily replenishment of media containing 2 μg/mL puromycin. Six days post-transduction, cells were plated into two sets of 8 15 cm dishes (96 million cells per set) for treatment and cell sorting the following day.

Cells at approximately 70% confluency were left untreated or treated for 8 hours with 50 nM ternatin-4. Cells were harvested by trypsinization, resuspended in FACS buffer (2% FBS, 100 U/mL penicillin, 100 μg/mL streptomycin, and 2 mM EDTA in PBS lacking Ca^{+2}/Mg^{+2}), and sorted on a BD FACS Aria II equipped with BD FACSDiva software. Single, BFP positive cells were separated into high, middle, and low thirds based on the calculated ratio of mCherry to GFP for each cell, with approximately 9 million cells collected for each population. Sorted cell populations were washed once with PBS and stored at -80°C until genomic DNA extraction.

Sorted samples were prepared for next-generation sequencing as previously described.[32] Briefly, genomic DNA was isolated from samples using the Machery-Nagel Blood Midi kit (catalog number 740954.20) according to the manufacturer's instructions. TSS (transcription start site)-specific sgRNA sequences were PCR amplified using all genomic DNA, indexed PCR primers, and 2x Q5 Hot Start PCR Master Mix (NEB M094). In total, approximately 40–55 60 μL PCR reactions were prepared for each sample. PCR products were size-selected using SPRI-select beads to remove PCR primers and genomic DNA, and samples were sequenced using an Illumina HiSeq 4000.

Individual sgRNA knockdown and rescue

Lentivirus was generated for plasmids encoding individual sgRNAs. CRISPRi reporter cells (ternatin-resistant HCT116 eEF1A1 A399V/A399V expressing Flag-mCherry-eEF1A1_IRES-AcGFP and dCas9-BFP-KRAB) were transduced, and sgRNA-expressing cells were selected three days post-transduction with 2 μg/mL puromycin for 48 hours. For RPS27A knockdown experiments, HeLa CRISPRi cells expressing RPS27A-3xFlag (sorted on the basis of GFP positivity after transduction with RPS27A-3xFlag_IRES-AcGFP), or CRISPRi mCherry-eEF1A reporter cells expressing RPS27A-3xFlag (~50% of cells as judged by iRFP positivity after transduction with RPS27A-3xFlag_IRES-iRFP), were transduced with sgRNA-encoding lentivirus and subjected to puromycin selection as above. For GCN1 rescue experiments, puromycin-selected, sgRNA-containing cells were transfected in 6-well dishes with 1 μg of the indicated GCN1 constructs (1 well/construct) using the manufacturer's protocol for Lipofectamine 2000 (Thermo Fisher).

The resulting cells were plated for experiments (typically 6 days post-transduction) in media lacking puromycin; the next day, cells were treated and analyzed as indicated in figure legends. For FACS-based analyses, cells were plated in 12-well dishes, and for immunoblotting experiments, cells were plated in 6-well dishes. For GCN1 rescue experiments, cells were plated approximately 24 hours post-transfection. For FACS-based experiments, following gating of debris and doublets, cells were gated on expression of sgRNAs (BFP positivity) and RPS27A or GCN1 (iRFP positivity), as applicable.

RT-qPCR

Cells were collected from 6-well dishes, washed once with cold PBS, and RNA was extracted using the RNeasy Mini Kit (Qiagen). cDNA was synthesized from 1 μg RNA per sample using the High-Capacity cDNA Reverse Transcription Kit (Applied Biosystems). 1/10th of each RT reaction was analyzed using Luna Universal qPCR Master Mix (NEB) according to the manufacturer's instructions and a BioRad CFX Touch Real-Time PCR instrument. mRNA abundance was quantified by the $\Delta\Delta C_q$ method, with GAPDH as the reference gene. Primer pairs for endogenous RPS27A or common to endogenous and transgenic RPS27A were designed using Primer Blast (NIH). The GAPDH primer pair was from the Harvard Medical School PrimerBank[73] (PrimerBank ID 378404907c2). Primer sequences were as follows.

RPS27A-endo_fwd: 5'-GGAGCCGCCACCAAAAT-3',
RPS27A-endo_rev: 5'-GCTTGCCAGCAAAGATCAGTC -3',
RPS27A-common_fwd: 5'-AGGCCAAGATCCAGGATAAGG-3',
RPS27A-common_rev: 5'-CACCACCACGAAGTCTCAACA-3',
GAPDH_fwd: 5'-ACAACTTTGGTATCGTGGAAGG-3',
GAPDH_rev: 5'-GCCATCACGCCACAGTTTC-3'

DiGly peptide enrichment

Cells were grown in light (Arg0/Lys0) or heavy (Arg10/Lys8) SILAC DMEM (Thermo Scientific) supplemented with 10% dialyzed FBS, 100 U/mL penicillin,100 μg/mL streptomycin, 80 μM lysine0 or lysine8, and 40 μM arginine0 or arginine10 for 12 days prior to indicated treatments. Typically, 5-6 15 cm dishes were used per label and treatment condition, yielding approximately 10-15 mg total protein. A label swap was performed as a biological replicate for all experimental conditions, except UV irradiation. Cells were harvested at room temperature by quickly aspirating media from dishes, rinsing once with ice-cold PBS, and scraping cells into cell lysis buffer (20 mM HEPES pH 8.0, 9 M urea, 1 mM sodium orthovanadate, 2.5 mM sodium pyrophosphate, 1 mM beta-glycerophosphate). Lysates were sonicated using three 15-second bursts from a microtip sonicator, and lysates were clarified by centrifugation at 19,000 g for 15 minutes at RT. Cleared lysates were quantified using the BCA method, and equal amounts of heavy and light samples were pooled (20-30 mg total). Samples were reduced with 4.5 mM DTT for 30 minutes at 55 °C. Samples were allowed to cool to room temperature and alkylated with 10.2 mM chloroacetamide for 30 minutes at RT. Lysates were diluted 4-fold with 20 mM HEPES pH 8.0 to a final concentration of approximately 2 M urea, sequencing-grade trypsin (Promega V5113) was added at a 1:300 w/w ratio, and samples were digested by rotating overnight at RT. The next day (approximately 18 hours later), trypsin digestion was stopped by addition of TFA to 1% final concentration. Samples were incubated on ice for 15 minutes and centrifuged at 1,780 g for 15 minutes at RT. Peptides were desalted using Waters 500 mg C18 SepPaks (WAT036945). SepPak cartridges were conditioned with 7 mL acetonitrile and equilibrated with 3 sequential washes of 1.4 mL, 4.2 mL, and 8.4 mL Solvent A (0.1% TFA in water) prior to loading of the clarified peptide solution. Peptides were loaded onto columns by gravity flow, and columns were washed 3 times using 1.4 mL, 7 mL, and 8.4 mL Solvent A. Peptides were eluted by 3 sequential additions of 2.8 mL solvent B (0.1% TFA, 40% acetonitrile in water). Samples were frozen and lyophilized for a minimum of 48 hours prior to immunoprecipitation of diGlycine-containing peptides.

Ubiquitin remnant-containing peptides were isolated using the Cell Signaling Technologies PTMScan Ubiquitin Remnant Motif Kit (CST #5562). Lyophilized peptides were collected by centrifugation at 2,000 g for 5 minutes at RT and dissolved in 1.4 mL ice-cold Immunoaffinity Purification (IAP) buffer (50 mM MOPS pH 7.2, 10 mM disodium phosphate, 50 mM NaCl). The peptide solution was cleared by centrifugation at 10,000 g for 5 minutes at 4 °C. The peptide supernatant was added to a tube containing immunoaffinity beads pre-washed 4x with 1 mL of cold PBS. All centrifugation steps with antibody beads were done at 2,000 g for 30 seconds at 4 °C. Immunoprecipitations were performed using a predetermined ratio of 10 mg input protein per 10 μL of antibody bead slurry.[74] Samples were rotated for 2 hours at 4 °C, and subsequently, peptide supernatant was removed from beads. Beads were washed twice with 1 mL ice-cold IAP buffer and 3 times with 1 mL ice-cold HPLC water. Peptides were eluted from beads with two consecutive incubations of 55 μL and 50 μL 0.15% TFA for 10 minutes at RT with gentle agitation every 2-3 minutes. Eluants were desalted using Agilent OMIX C18 tips (A57003100), dried by vacuum concentration, and stored at -80 °C until analysis.

LC-MS/MS data acquisition (DDA)

One half of each sample was resuspended in 10 μL 0.1% FA or 10 μL 0.1% FA containing 2.5 nM eEF1A K385 standard peptide (SGK [diGly]KLEDGPK, with $^{13}C_6$, ^{15}N-Leu). One quarter of each reconstituted sample (2.5 μL; 12.5% of total sample) was analyzed on an Orbitrap Fusion Lumos (Thermo Scientific) equipped with an ACQUITY M-Class UPLC (Waters) and an EASY-Spray C18 column (Thermo Scientific #ES800; 75 μm x 15 cm, 3 μm particle size, 100 Å pore size). Solvent A was 0.1% FA in water, and Solvent B was 0.1% FA in acetonitrile. Peptides were loaded onto the warmed column (45 C), and equilibrated with 0% B for 13 min using a flow rate of 600 nL/min, followed by 0-30% B over 120 min at 300 nL/min, 30-80% B over 20 min, 80% B for 5 min, 80%-0% B over 2 min, and 0% B for 10 min with the flow rate changed back to 600 nL/min. The entire method ran for a total of 170 min. Mass spectra were acquired in data dependent mode. MS1 scans were collected in the orbitrap at a resolution of 120,000, a scan range of 375-1500 m/z, an automatic gain control (AGC) target of 4E5, and a maximum injection time of 50 ms. Ions with a

peptide-like isotopic distribution (MIPS set to "peptide") that exceeded an intensity threshold of 2E4 and contained a charge between 2 and 7 were selected for HCD fragmentation. MS2 spectra of HCD-fragmented peptides were collected using a 1.6 m/z isolation window and an HCD collision energy of 30%. Fragment ions were measured in the orbitrap at a resolution of 30,000 and were collected with an AGC target of 5E4 and a maximum injection time of 100 ms. Peptides selected for fragmentation were dynamically excluded for the following 30 seconds using a 10-ppm window. The maximum duty cycle was set to 3 s.

PRM analysis of eEF1A K385 ubiquitination

Sample reconstitution and liquid chromatography proceeded identically to DDA preparations (see above). For each cycle of the PRM method, an MS1 scan was first collected with a scan range of 360–1300 m/z, a resolution of 60,000, an automatic gain control (AGC) target of 4E5, and a maximum injection time of 50 ms. Subsequently, targeted MS2 scans were collected for heavy, light, and standard (medium) eEF1A K385 peptides (z = 3; m/z = 399.5614, 391.5472, and 393.8862, respectively). MS2 precursors were fragmented by HCD using a collision energy of 30%. MS2 scans utilized an isolation window of 0.7 m/z, a resolution of 15,000, an AGC target of 1E5, and a maximum injection time of 150 ms. The entire scan cycle was repeated over the entire gradient. Data was analyzed with Skyline using a reference library constructed from previous DDA runs with the same samples. The six most highly ranked (most intense) b or y ions were chosen for generation of extracted ion chromatograms.

Proximity-based ubiquitination assay

Ternatin-resistant HCT116 cells (eEF1A1 A399V/A399V) stably expressing 3xFlag-eEF1A were cultured in DMEM, which does not contain biotin, supplemented with 10% fetal bovine serum. The assay was based on Deshar et al.,[43] with some modifications. Cells were grown to 70% confluency in 10 cm dishes and were co-transfected with 1.8 μg AP-HA-Ub (pcDNA3.1) and 8.8 μg V5-BirA or V5-BirA-RNF (pHR) constructs using the manufacturer's protocol for Lipofectamine 2000. The next day, cells were treated with 50 μM biotin and with DMSO or 50 nM ternatin-4 for 4 h. For analysis of RPS27A ubiquitination, Hela cells stably expressing RPS27A-3xFlag were grown to 70% confluency in 15 cm dishes, co-transfected with 2 ug AP-HA-Ub and 8 ug V5-BirA constructs using the manufacturer's protocol for Lipofectamine LTX, and treated the next day with 50 μM biotin and DMSO or 50 nM ternatin-4 for 1 h.

Following treatment, cells were washed once with ice-cold PBS and collected by scraping into PBS. Cells were centrifuged at 1000 g for 3 minutes at 4 °C, and cell pellets were frozen in liquid nitrogen and stored at -80 °C or immediately lysed. Cells were lysed in lysis buffer (50 mM HEPES pH 7.4, 150 mM NaCl, 1% NP-40, 2x Roche EDTA-free protease inhibitors, and 50 mM chloroacetamide) and lysate was cleared by centrifugation at 16,100 g for 10 minutes at 4 °C. SDS was added to supernatants to 1% final concentration, and samples were boiled for 10 minutes. Denatured lysates were quantified by the Bradford method, normalized, and diluted 10-fold in lysis buffer. Diluted lysates were filtered through 0.45 μm SFCA syringe filters (Thermo Scientific) and were added to tubes containing streptavidin magnetic beads (Pierce; 40 μL beads per 1 mg protein). Samples were rotated for 2 hours at 4 °C. Supernatants were removed from beads, and beads were washed twice with wash buffer 1 (50 mM HEPES pH 7.4, 150 mM NaCl, 1% NP-40, 0.1% SDS), and twice with wash buffer 2 (50 mM HEPES pH 7.4, 500 mM NaCl, 1% NP-40). Bound proteins were eluted by boiling beads for 10 minutes in elution buffer (50 mM HEPES pH 7.4, 150 mM NaCl, 1% NP-40, 5 mM biotin, and 1x SDS loading buffer). 10 μg of input protein (typically < 3% total input protein) and 40% of eluants were loaded on 7.5% gels and analyzed by immunoblotting.

K6-linked ubiquitin enrichment

HeLa RNF14 KO or rescue cells were grown to approximately 70% confluency in 15 cm dishes prior to treatment. Cells were harvested by scraping into ice-cold PBS and centrifuged at 1000 g for 3 minutes at 4 °C. Cells were lysed in lysis buffer (50 mM HEPES pH 7.4, 150 mM NaCl, 1% NP-40, 2x Roche EDTA-free protease inhibitors, 5 mM EDTA, and 50 mM chloroacetamide) and lysates were cleared by centrifugation at 16,100 g for 10 minutes at 4 °C. The K6-ubiquitin affimer[52] (linked to GFP), was added to lysates (1 μg affimer per 1 mg lysate) as indicated and rotated for 2 hours at 4 °C. GFP-Trap beads (ChromoTek; 5 μL per sample) were added to samples and rotated for an additional 2 hours at 4 °C. Supernatants were removed from beads, and beads were washed twice with wash buffer 1 (50 mM HEPES pH 7.4, 150 mM NaCl, 1% NP-40, 5 mM EDTA), and twice with wash buffer 2 (50 mM HEPES pH 7.4, 500 mM NaCl, 1% NP-40, 5 mM EDTA). Bound proteins were eluted by boiling beads for 10 minutes in elution buffer (50 mM HEPES pH 7.4, 150 mM NaCl, 1% NP-40, 5 mM EDTA, and 1x SDS loading buffer). 10 μg of input protein (1-2% total input protein) and 33% of eluants were loaded on 4-12% Bis-Tris gradient gels (Invitrogen) gels and analyzed by immunoblotting.

Co-immunoprecipitations

For GCN1-3xFlag immunoprecipitations, HEK293T cells growing in a 15 cm dish at approximately 70% confluency were transfected with 8 μg plasmid (pLenti6.3) using Lipofectamine 2000. The next day, cells were split between two 15 cm dishes. Cells were treated approximately 48 hours post-transfection. For 3xFlag-RNF14 or RNF25 immunoprecipitations, HeLa cells stably expressing the indicated construct were were grown to approximately 70% confluency and treated in 10 cm dishes.

Cells were harvested by scraping into ice-cold PBS and centrifuged at 1000 g for 3 minutes at 4 °C. Unless otherwise indicated, cells were crosslinked as previously described[75]: cells were resuspended in 1 mL PBS containing 0.1% PFA (Electron Microscopy Sciences) and were rotated for 10 minutes at room temperature; crosslinking was stopped by addition of 100 μL quench solution (2.5 M glycine, 25 mM Tris pH 7.4), and cells were centrifuged at 1000 g for 3 minutes at 4 °C. Cells were lysed in lysis buffer

(50 mM HEPES pH 7.4, 100 mM KOAc, 5 mM $Mg(OAc)_2$, 0.1% NP-40, 40 U/mL RNase inhibitor (NEB), 2x Roche EDTA-free protease inhibitors, and 50 mM chloroacetamide) for 5 minutes on ice, and lysates were cleared by centrifugation at 15,000 g for 10 minutes at 4 °C. Lysates were quantified by the Bradford method and normalized. Samples were added to tubes containing Flag M2 magnetic beads (Sigma) and rotated for 1 hour at 4 °C. For GCN1-3xFlag IPs, 40 μL bead slurry was used per 1 mg protein, and for 3xFlag-RNF14 and RNF25 IPs, 20 μL bead slurry was used per 1 mg protein. After binding, supernatants were removed and beads were washed 3 times using wash buffer (50 mM HEPES pH 7.4, 100 mM KOAc, 5 mM $Mg(OAc)_2$, 0.1% NP-40). Two sequential elutions were performed by incubating 200 μg/mL 3xFlag peptide in wash buffer with rotation for 30 minutes at 4°C. 10 μg input protein (typically < 2% total input protein) and 40% of IP eluates were loaded onto 4%–12% Bis-Tris gradient gels (Invitrogen) and analyzed by immunoblotting.

Sucrose density gradient ultracentrifugation

HeLa cells were grown to approximately 80% confluency in 15 cm dishes prior to treatment. Cells were harvested by scraping into ice-cold PBS and were centrifuged at 1000 g for 3 minutes at 4 °C. Cells were lysed (50 mM HEPES pH 7.4, 100 mM KOAc, 15 mM $Mg(OAc)_2$, 0.1% NP-40, 5 U/mL Turbo DNAse (Invitrogen), 20 U/mL SUPERaseIn (Invitrogen), 2x Roche EDTA-free protease inhibitors, and 50 mM chloroacetamide) for 5 minutes on ice. For samples intended for nuclease digestion, SUPERaseIn was omitted from the lysis buffer. Lysates were cleared by centrifugation at 15,000 g for 10 minutes at 4 °C, and supernatants were normalized based on NanoDrop (Thermo Scientific) readings at 260 nm (typically 60 – 120 μg RNA). Where indicated, RNA was digested as follows: $CaCl_2$ was added to a final concentration of 1 mM, 20 U micrococcal nuclease (Roche) was added per 40 μg RNA, and samples were shaken (500 rpm) on a Thermomixer for 45 minutes at RT. Digestion was quenched by adding EGTA to a final concentration of 2 mM, and 12 U SUPERaseIn was added per 40 μg RNA.

Prepared samples were layered onto 10-50% sucrose gradients for polysome analysis, and 10-40% or 10-50% gradients for analysis of nuclease-digested samples, as indicated. All gradients were composed of 50 mM HEPES pH 7.4, 100 mM KOAc, and 15 mM $Mg(OAc)_2$, and were formed using a Biocomp Gradient Station. Samples were resolved by ultracentrifugation through gradients using an SW-41 rotor (Beckman Coulter) spun at 4 °C for 3 hours at 35,000 rpm. Samples were fractionated (typically 930 μL per fraction) and absorbance at 260 nm was monitored using a Biocomp fractionator and a Triax flow cell. Equal amounts of each fraction (typically 10 μL) were loaded onto 4-12% Bis-Tris gradient gels (Invitrogen) and analyzed by immunoblotting.

QUANTIFICATION AND STATISTICAL ANALYSIS

Quantification and normalization

Immunoblots were visualized using a Li-Cor Odyssey near-IR system. The resulting images were quantified using Image Studio Lite (Li-Cor). Where indicated, intensities were normalized to vehicle controls. Flow cytometry data was quantified using the mean fluorescent intensity (MFI; protein synthesis measurements), or median mCherry/GFP ratio (eEF1A degradation reporter), across a single cell population. MFI values were normalized to the vehicle control for an indicated cell line. A minimum of two independent replicates were performed with similar results for immunoblotting and flow cytometry experiments.

CRISPRi screen analysis

Sequencing data was analyzed as previously described.[31,32] Briefly, raw sequencing data was aligned to the reference library sequences using Bowtie, and the number of reads for each sgRNA were counted. Sequencing counts were normalized to the total number of counts within each sequenced sample. Phenotype scores for each sgRNA were calculated as the log_2 ratio of high mCherry/GFP sequencing counts divided by low mCherry/GFP counts. An epsilon value was calculated by averaging the three most extreme phenotype scores for each transcription start site (TSS). A p value for each TSS was calculated using the Mann-Whitney U test against nontargeting controls. A gene score was calculated for each TSS as the product of the epsilon score and the $-log_{10}$(p value). Epsilon values, p values, and products for all genes targeted in the library are included in Table S1.

Mass spectrometric site identification and quantification

The raw data were searched against the human Uniprot database (73,651 entries) using MaxQuant (version 1.6.7.0) with a list of common laboratory contaminants added. 'Arg10' and 'Lys8' were selected as heavy labels. The digestion enzyme was set to trypsin, a maximum of three missed cleavages were allowed, and the minimum peptide length was set to 7. Cysteine carbamidomethylation was specified as a fixed modification, and N-terminal protein acetylation and methionine oxidation were set as variable modifications. Internal lysine diGlycine modifications, and lysine diGlycine modifications at the protein C-terminus were additionally set as variable modifications. The remainder of the search parameters were left at default settings. Peptide requantification was enabled for calculation of H/L SILAC ratios. DiGly site identifications and normalized SILAC ratios were obtained from the MaxQuant sites file. SILAC ratios were inverted for label swap experiments. Site values were averaged between biological replicates, log_2-transformed, and reported in Table S2.
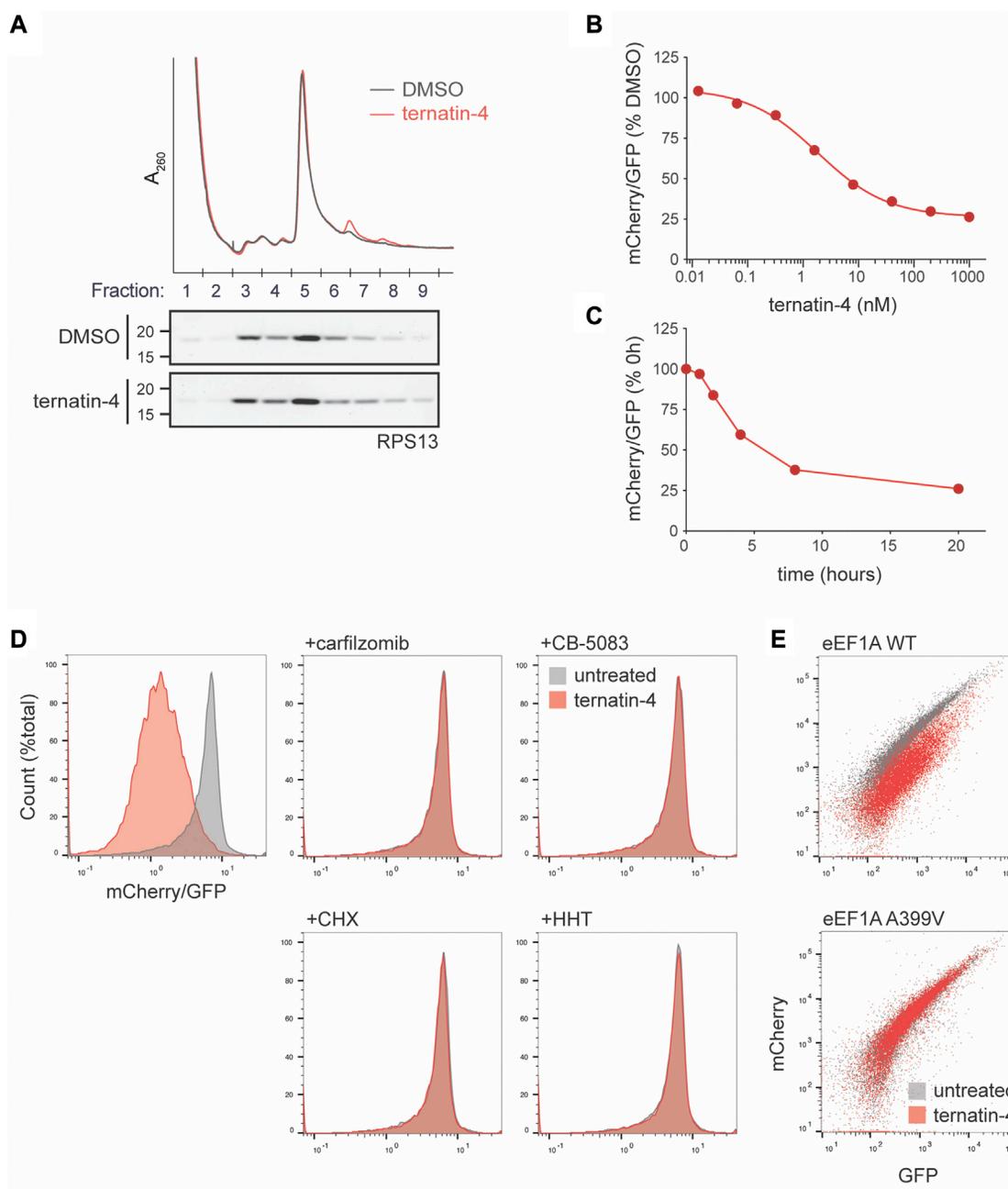
Supplemental figures

Figure S1. Ternatin-4 promotes eEF1A degradation in a manner that requires translating ribosomes, related to Figure 1

(A) HeLa cells were treated with ternatin-4 (50 nM) for 1 h. Lysates were digested with micrococcal nuclease and subjected to ultracentrifugation through 10%–50% sucrose gradients. Ribosome abundance was measured by monitoring absorbance throughout the gradient at 260 nm and immunoblotting for RPS13.

(B) Dose-dependent mCherry-eEF1A reporter degradation. Ternatin-resistant HCT116 cells stably expressing the FLAG-mCherry-eEF1A1_IRES-GFP reporter and dCas9-BFP-KRAB were treated with 50 nM ternatin-4 for 8 h and analyzed by flow cytometry.

(C) Time dependence of mCherry-eEF1A reporter degradation. Cells as in (B) were treated with 50 nM ternatin-4 for the indicated times and analyzed by flow cytometry.

(D) Cells in each panel were treated ±ternatin-4 (50 nM) for 8 h, along with carfilzomib (500 nM), CB-5083 (2.5 μM), CHX (50 μg/mL), or HHT (2 μg/mL, 20 min pretreatment), as indicated.

(E) Cells expressing WT or A399V mCherry-eEF1A were treated ±ternatin-4 (50 nM) for 8 h and analyzed by flow cytometry.
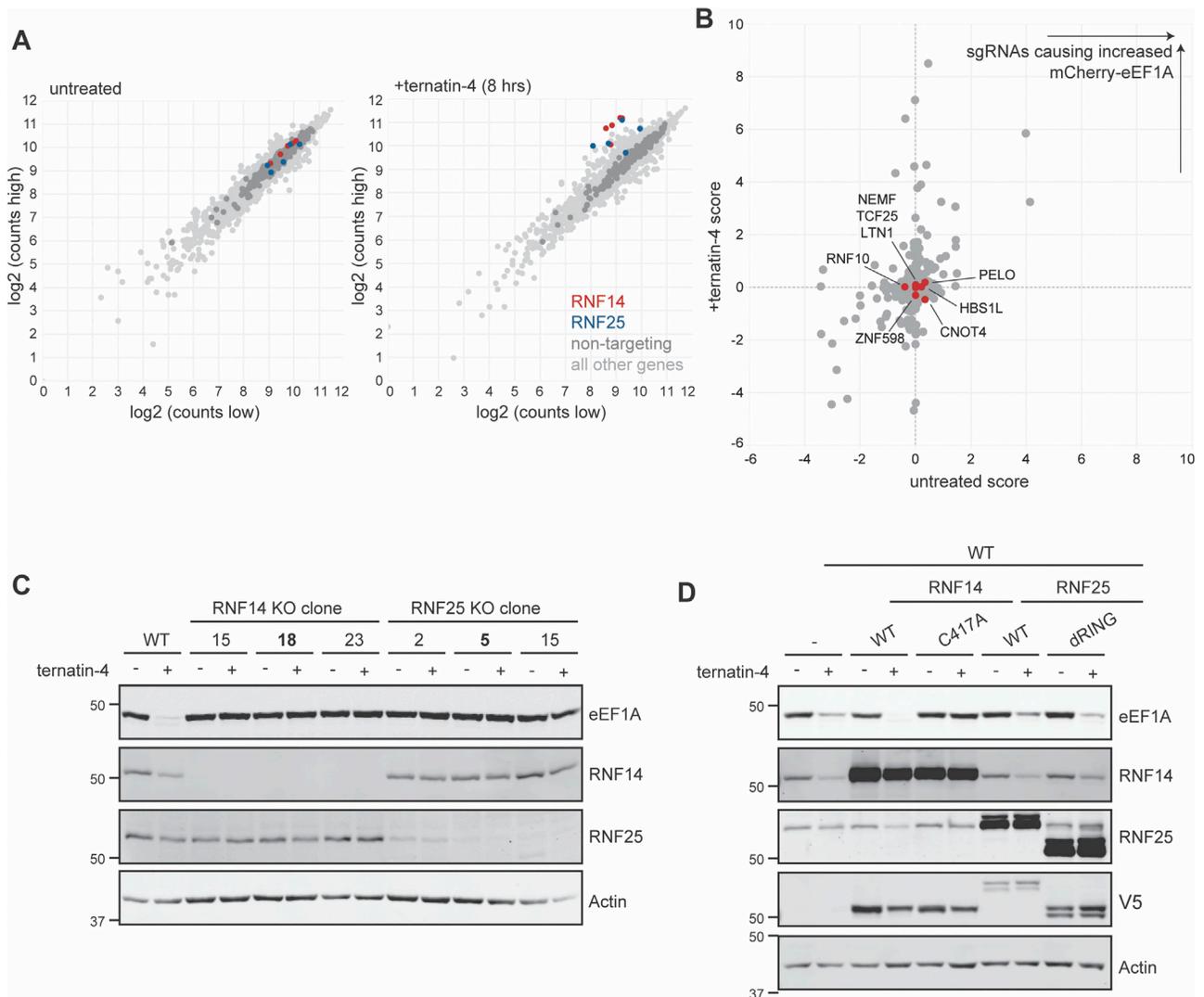
Figure S2. CRISPRi screen reveals two E3 ligases required for ternatin-induced eEF1A degradation, related to Figure 2

(A) sgRNA sequencing counts for high and low fluorescence cell populations (±ternatin-4) from the CRISPRi screen, highlighting RNF14 and RNF25 sgRNAs.

(B) CRISPRi scores from Figure 2B are shown in red for HBS1L, PELO, LTN1, ZNF598, NEMF, RNF10, and CNOT4.

(C) Knockout of RNF14 or RNF25 prevents ternatin-induced eEF1A degradation across multiple HeLa cell clones. Cells were treated with ternatin-4 for 20 h and analyzed by immunoblotting. Clones 18 (RNF14) and 5 (RNF25) were utilized for further experiments.

(D) Overexpression of V5-tagged RNF14, but not RNF25, increases eEF1A degradation in wild-type HeLa cells. Stable cell lines were generated as in Figure 2E and treated for 20 h with ternatin-4.
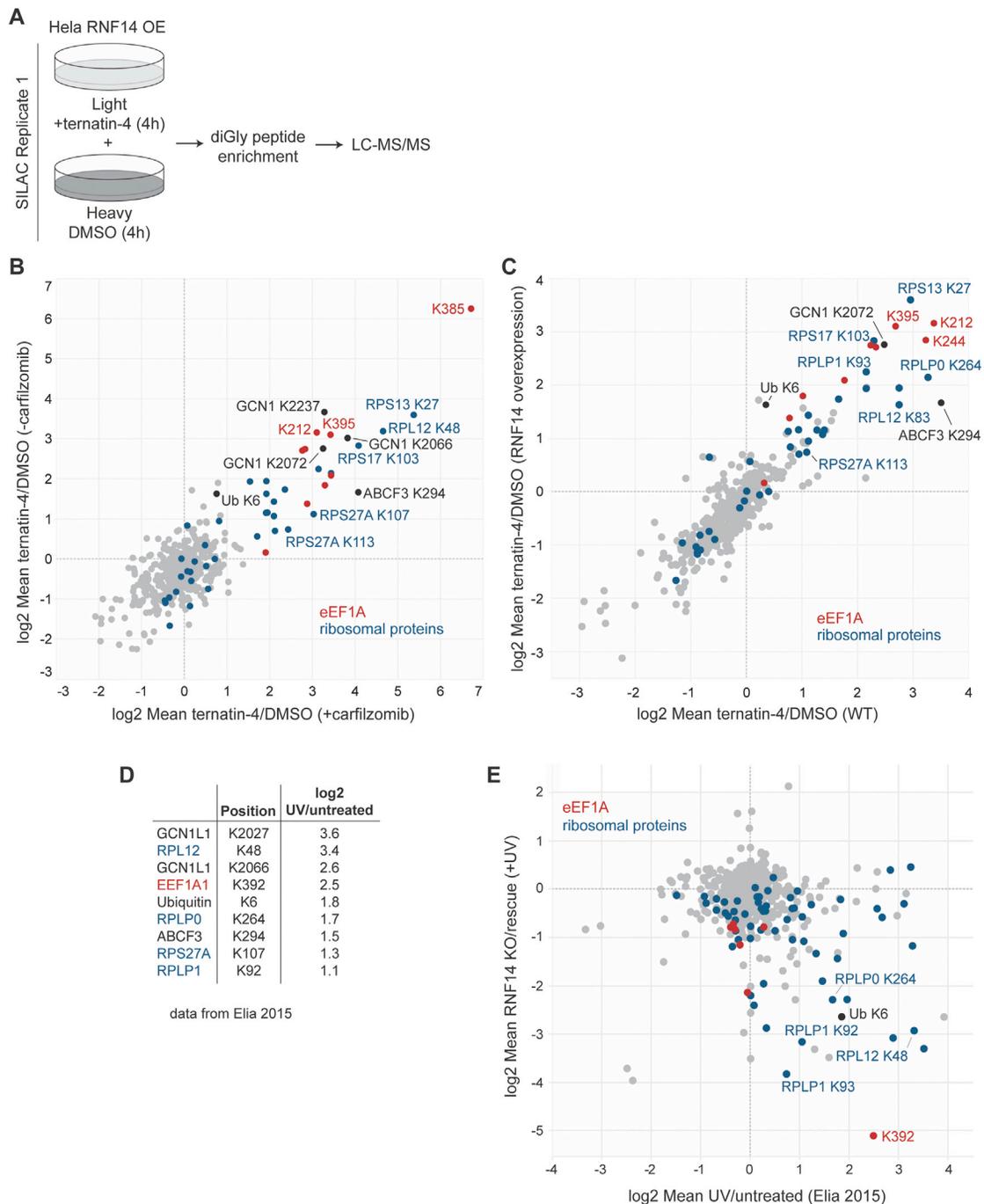
Figure S3. Ternatin-4 promotes RNF14 and RNF25-dependent ubiquitination of eEF1A and ribosomal proteins, related to Figure 3

(A) Schematic for the SILAC-based diGly proteomics method to identify ternatin-induced ubiquitination sites. Sample configuration is shown for the experiment in Figures 3A and 3B. Replicate 2 was performed identically except heavy and light labels (Arg/Lys in growth media) were swapped.

(B) HeLa cells stably overexpressing RNF14 were labeled in SILAC media as in (A) and treated with 500 nM carfilzomib ±ternatin-4 (50 nM) for 4 h. Mean SILAC ratios (log$_2$) for each ubiquitination site (2 replicates, label swaps) were plotted against corresponding log$_2$ ratios from the experiment shown in Figures 3A and 3B (without carfilzomib).

(C) HeLa cells (without RNF14 overexpression) were labeled in SILAC media as in (A) and treated ±ternatin-4 (50 nM) for 4 h. Mean SILAC ratios (log$_2$) for each ubiquitination site (2 replicates, label swaps) were plotted against the corresponding log$_2$ ratios from the experiment shown in Figures 3A and 3B (HeLa RNF14 OE).

(legend continued on next page)

(D) Published SILAC diGly proteomics data[39] derived from HeLa cells irradiated with UV light (40 J/m^2) and then allowed to recover for 1 h. UV-induced diGly sites (log$_2$ SILAC ratio >1) also induced by ternatin-4 are tabulated (UV/untreated, mean of 3 replicates).

(E) Comparison of UV-induced ubiquitination sites[39] and ubiquitination sites from HeLa RNF14 KO and rescue cells both irradiated with UV light (40 J/m^2) and allowed to recover for 1 h. UV-induction data[39] are shown as the log$_2$ UV/untreated ratio from the mean of three biological replicates. RNF14 KO vs. rescue data are shown as the log$_2$ (KO/rescue) ratio from the mean of three technical replicates.
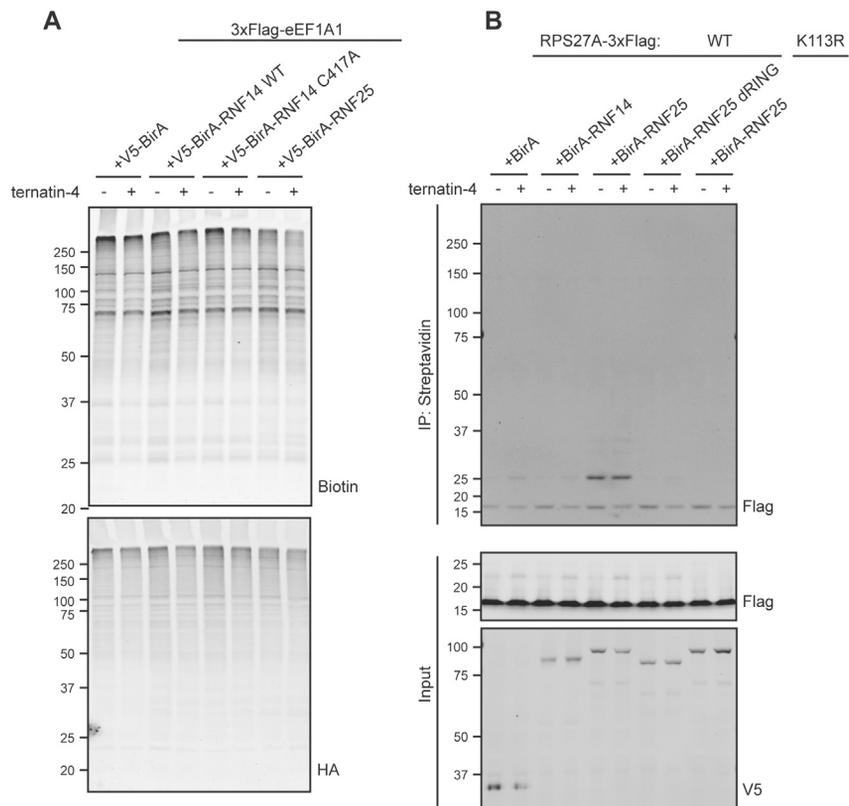
Figure S4. eEF1A K385 is required for efficient degradation and is directly ubiquitinated by RNF14, related to Figure 4

(A) Cell lysates from Figure 4D were analyzed by immunoblotting for AP-HA-Ub (anti-HA) and biotinylated proteins (streptavidin).

(B) HeLa cells stably expressing WT or K113R RPS27A-3xFLAG were transfected with AP-HA-Ub and the indicated V5-tagged BirA constructs. Cells were treated with 50 μM biotin ± ternatin-4 (50 nM) for 1 h, and biotinylated products were subsequently enriched and analyzed by immunoblotting as in Figure 4.
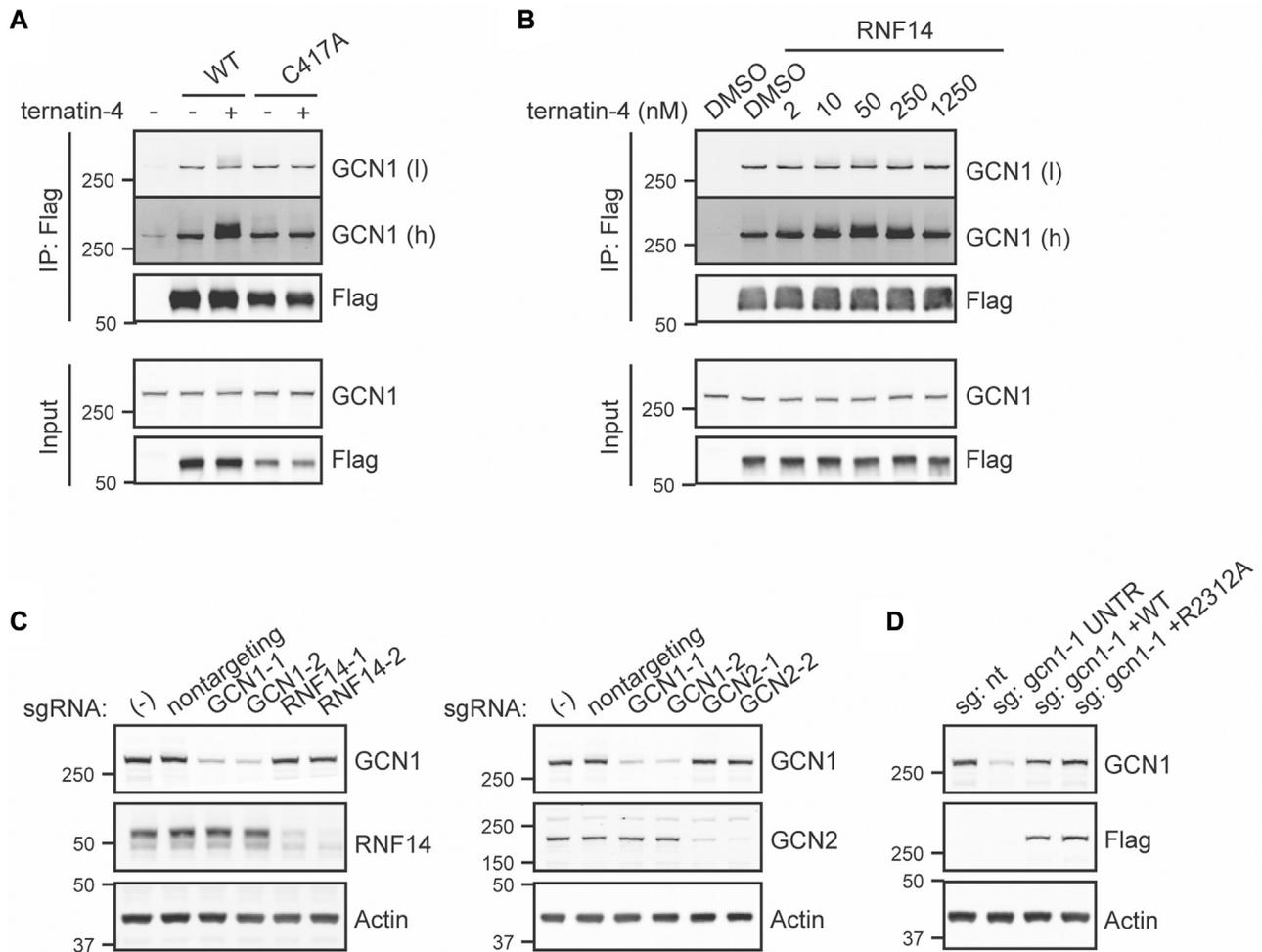
Figure S5. GCN1 interacts with RNF14 and is essential for ternatin-induced eEF1A degradation, related to Figure 5

(A) Ternatin-induced GCN1 modification requires the catalytic cysteine (C417) of RNF14. As in Figure 5A, HeLa WT cells stably expressing WT or C417A 3xFLAG-RNF14 were treated with ternatin-4 (50 nM) for 4 h prior to crosslinking with 0.1% PFA, FLAG immunoprecipitation, and immunoblotting. Low- and high-intensity immunoblot images for GCN1 are shown to indicate higher-MW, presumably multi-ubiquitinated forms of GCN1.

(B) HeLa WT cells stably expressing 3xFLAG-RNF14 were treated with the indicated concentrations of ternatin-4 for 1 h. Samples were crosslinked with 0.1% PFA prior to FLAG immunoprecipitation and immunoblotting as in (A).

(C) Immunoblot analysis of lysates from sgRNA-expressing cells used in Figure 5C. Cells were puromycin selected and collected 8 days after sgRNA trans-duction. All samples were prepared from the same experiment but are depicted on different blots.

(D) WT and R2312A GCN1 rescue constructs are expressed at similar levels. Cells puromycin selected for sgRNA expression were transfected with the indicated GCN1-3xFLAG_IRES-iRFP constructs to give ~20% iRFP+ cells. Lysates from the untreated cells used in Figure 5D were analyzed by immunoblotting to show knockdown of endogenous GCN1 and overexpression of exogenous WT and R2312A GCN1-3xFLAG.
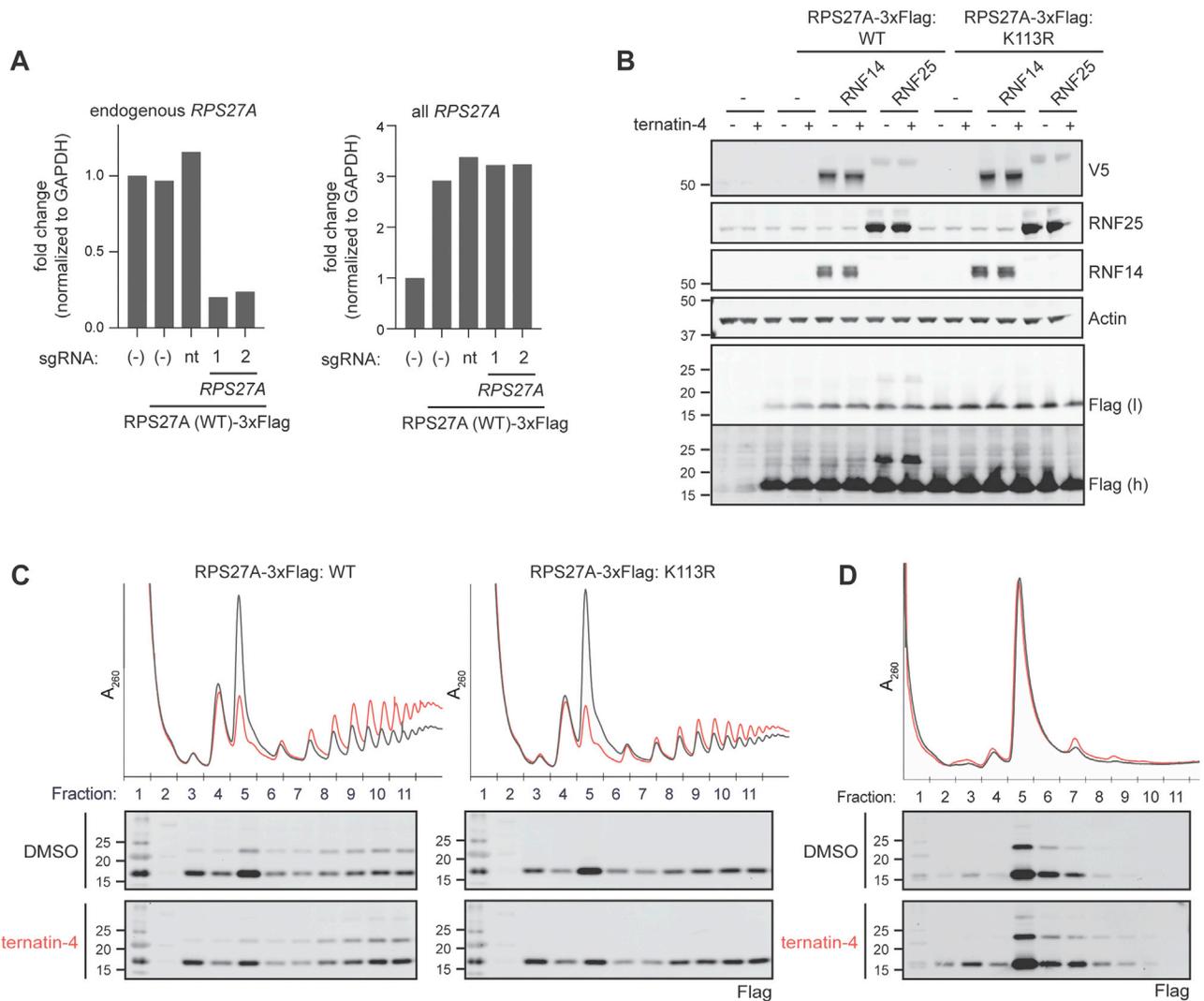
Figure S6. Ubiquitination of RPS27A/eS31 K113 is essential for eEF1A degradation, related to Figure 6

(A) Cells from Figure 6A (pure populations of HeLa CRISPRi cells expressing RPS27A-3xFLAG and the indicated sgRNAs) were subjected to qPCR analysis for endogenous *RPS27A*, both endogenous and exogenous *RPS27A*, or *GAPDH*. *RPS27A* mRNA levels were normalized to *GADPH* expression and are plotted relative to parental HeLa CRISPRi cells. Note that the CRISPRi system targets the endogenous *RPS27A* transcriptional start site (not the *RPS27A* coding sequence), thus allowing the expression of exogenous RPS27A.

(B) HeLa CRISPRi cells stably expressing WT or K113R RPS27A-3xFLAG and V5-RNF14 or RNF25 were treated with ternatin-4 for 1 h and analyzed by immunoblotting.

(C) HeLa cells stably expressing V5-RNF25 and WT or K113R RPS27A-3xFLAG were treated with ternatin-4 for 1 h. Lysates were resolved by ultracentrifugation through 10%–50% sucrose gradients, analyzed by A260, and fractionated. Equal amounts of each fraction were analyzed by immunoblotting.

(D) HeLa cells stably expressing V5-RNF25 and WT RPS27A-3xFLAG were treated with ternatin-4 for 1 h. Lysates were digested with micrococcal nuclease prior to fractionation through 10%–40% sucrose gradients and analysis as in (C).
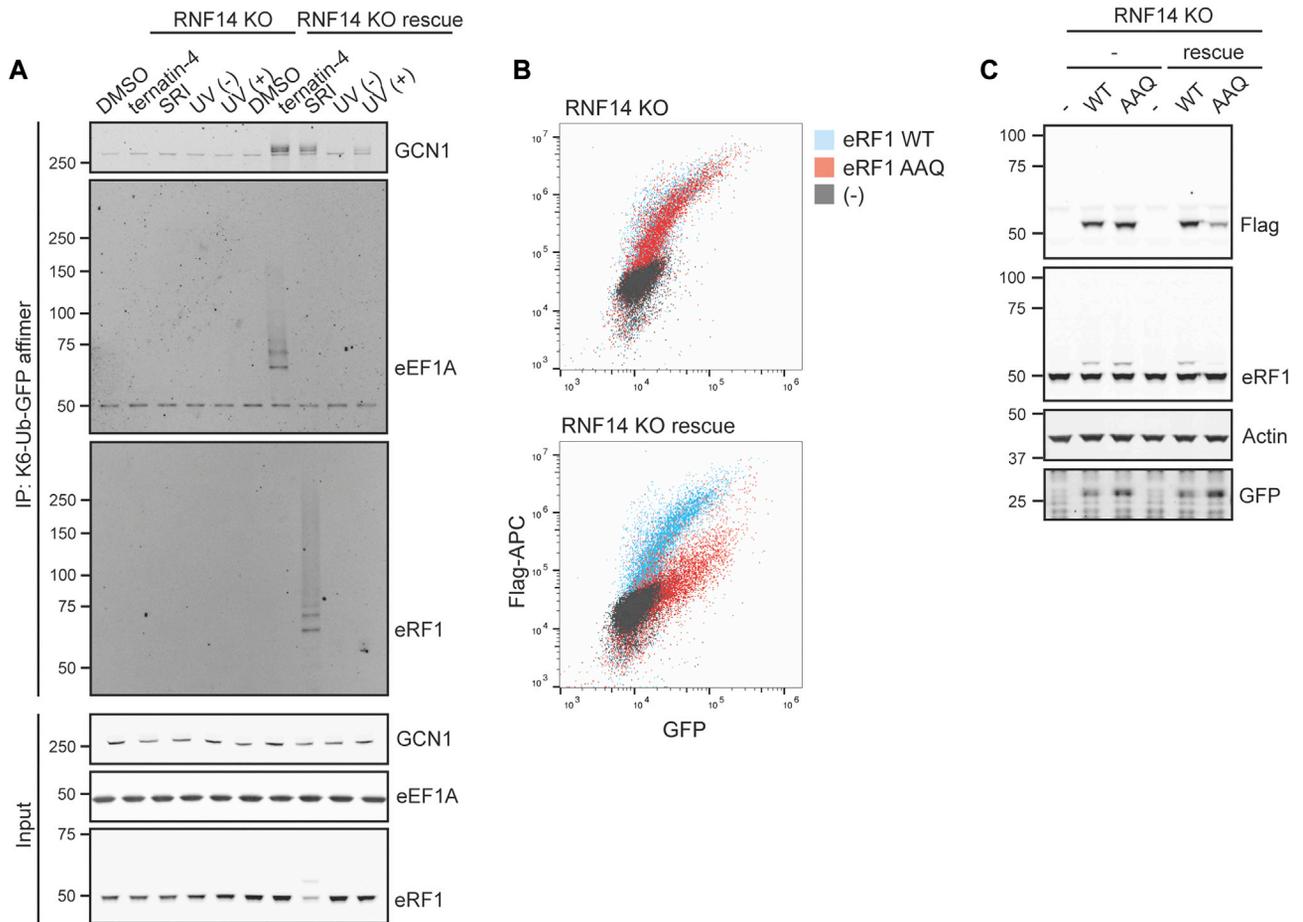
Figure S7. RNF14 and RNF25 promote degradation of the termination factor eRF1, related to Figure 7

(A) HeLa RNF14 KO or rescue cells were treated with DMSO, ternatin-4, or SRI-41315 for 1 h or were irradiated ±40 J/m² UV and allowed to recover for 1 h. Cell lysates were enriched for K6-linked ubiquitin conjugates as in Figure 7C and analyzed by immunoblotting.

(B) Flow cytometry scatter plots depicting anti-FLAG-APC and GFP for the cells displayed in Figure 7D.

(C) Cells transduced with WT or AAQ eRF1 (IRES-GFP) as in Figure 7D were analyzed by immunoblotting.